JOINT EUROPEAN TORUS JET

JET–P(93)18

B. Balet, P.M. Stubberfield, D. Borba, J.G. Cordey, N. Deliyanakis,
C.M. Greenfield, T.T.C. Jones, R. König, F.B. Marcus, M.F. Nave,
D.P. O'Brien, F. Porcelli, G. Sadler, K. Thomsen, M. von Hellermann

Particle and Energy Transport during the First Tritium Experiments on JET

Particle and Energy Transport during the First Tritium Experiments on JET

B. Balet, P.M. Stubberfield, D. Borba[1], J.G. Cordey, N. Deliyanakis, C.M. Greenfield[2], T.T.C. Jones, R. König, F.B. Marcus, M.F. Nave[1,3], D.P. O'Brien, F. Porcelli, G. Sadler, K. Thomsen, M. von Hellermann

JET-Joint Undertaking, Culham Science Centre, OX14 3DB, Abingdon, UK

[1]Associacao Euratom/IST, Centro de Fusao Nuclear, Instituto Superior Technico, Lisbon Codex, Portugal.
[2]General Atomics, San Diego, CA 92186, USA.
[3]Laboratorio Nacional de Engenharia e Technologia Industrial, Lisbon, Portugal.

Preprint of a paper to be submitted for publication in Nuclear Fusion
March 1993

ABSTRACT

The particle and energy transport properties of the high fusion performance JET pulses that were obtained before and during the first tritium experiments are discussed. The particle diffusion coefficient of tritium is determined by monitoring the decay of a small quantity of injected tritium in a deuterium background plasma. A good simulation of the measured 14 MeV emissivity profile is obtained throughout the decay phase, if the mixing of the two species is described by a model in which the tritium diffusion coefficient is similar to that of the deuterium. The energy confinement of these low density hot-ion H-mode discharges is found to have both improved central and edge confinement over the conventional medium to high density H-mode discharges. Enhancement factors of at least twice the value predicted by H-mode scaling expressions are observed transiently. A local transport analysis is completed to try and establish the reason for the improved confinement. Several possibilities are investigated, including stabilisation of the η_i mode by the peaked density profile and access to the second ballooning mode stable region. Finally, for the discharge with a high concentration of tritium, it has been suggested that α-particle driven instabilities could affect the energy confinement. A comparison is made with the stability threshold of toroidicity induced Alfvén eigenmodes (TAE) and the α-particle statistics are presented.

1. INTRODUCTION

During 1989 - 1990, several high performance low density hot ion ($T_i > T_e$) H-mode deuterium plasmas were obtained in JET, producing Q_{DD} values of about 2×10^{-3} with the instantaneous neutron emission rate exceeding 3.5×10^{16} /s [1]. Extrapolations of these high performance discharges to D-T operation were performed using the TRANSP code [2]. They showed that, assuming the same plasma conditions that had been achieved with deuterium, fusion yields in the range of 9 to 12 MW with a Q_{DT} between 0.6 to 0.8 could be obtained for a 50 : 50 D-T mixture [3]. These results meant that a worthwhile D-T experiment could be performed with a smaller tritium concentration (~ 10%): such an experiment took place in November 1991 [4]. The plasma chosen for this experiment was in the hot ion H-mode regime with a total plasma current of 3.1 MA and a toroidal magnetic field of 2.8 T. It was a single null X-point discharge, diverted onto the upper carbon target, with the toroidal magnetic field direction causing the ions to drift away from the target and towards the plasma. Such a

configuration leads to a more equal power loading between the inner and outer strike zones on the X-point target [5] and consequently allows higher energy input and longer duration of the high performance phase before a large influx of impurities occurs. Several extrapolations using the TRANSP code were performed to determine the most fuel efficient high performance scenario. These predictions together with the limited amount of tritium available (0.2g ~ 2000 Ci) implied that the introduction of tritium should be as energetic neutrals. This was the first time that a neutral beam system had been used to inject tritium and represented an important advance in this technology. Furthermore the predicted performance of D-T plasmas where the tritium is introduced as energetic neutrals is relatively insensitive to the model used to separate the flows of each of the two hydrogenic species (the mixing model, see Section 2). By contrast, in plasmas where the tritium is introduced by gas puffing, the estimated performance is strongly dependent on the mixing model assumptions.

The First Tritium Experiments in JET were carried out in the following steps:

1) Operation with deuterium alone to set up the target plasma and to test its performance and relative insensitivity to small changes (such as the level of injected power). Amongst these high performance shots, the deuterium discharge, pulse no. 26087, achieved the best maximum instantaneous total neutron emission rate of 4.3×10^{16} /s and a fusion triple product $n_D T_i \tau_E = 9 \times 10^{20}$ m^{-3} keV s.

2) A series of discharges in which one or two of the neutral beam sources (out of sixteen) were fuelled with 1% tritium in deuterium, to verify the operational procedures and to test the diagnostics. Good agreement was obtained between the measured and simulated neutron emission rates for both 2.5 MeV and 14 MeV neutrons confirming the consistency of the data and the TRANSP simulation. Extrapolations using TRANSP were then used to optimise the pre-fuelling scenario of the final phase. Tritium decay experiments were also performed in conventional medium density ($T_i = T_e$) H-mode plasmas during this phase to determine the particle transport of thermalised tritium and deuterium.

3) Two discharges into which two of the neutral beam sources injected tritium. The second of the two tritium shots, pulse no. 26148, achieved a peak

instantaneous neutron emission rate of 6×10^{17} /s corresponding to a fusion power of 1.7 MW [4].

4) "Clean-up" experiments in which the efficiency of different scenarios to remove the tritium from the torus were tested [6].

The aim of this paper is to describe and discuss the particle and energy transport in this series of experiments. Several of these discharges have been extensively analysed by TRANSP. The input data to the code was as follows: the profiles of the electron temperature T_e (from Electron Cyclotron Emission measurements), of the ion temperature T_i, rotation velocity V_ϕ and effective charge Z_{eff}, based on the measurement by charge exchange recombination spectroscopy of the dominant low Z impurities C, Be and He, and of the electron density n_e (from far infra-red interferometer). The electron temperature T_e and density n_e profiles were cross-checked by Lidar Thomson scattering measurements. Monte-Carlo techniques are used to simulate the neutral beam heating processes. The consistency of the input data was checked by comparing the measurement and simulation of the diamagnetic and MHD energies, the loop voltage and, most importantly, the total neutron yield and profile (from the neutron emission profile monitor, fission chambers and silicon diodes). Examples of such consistency checks are shown in Fig. 1 for the best deuterium discharge, pulse no. 26087. The quoted errors on the derived quantities from TRANSP have been determined in the manner described previously [7].

TRANSP can estimate the fraction of neutrons produced by thermal-thermal, beam-thermal and beam-beam reactions as well as simulating the birth and slowing down of the different fusion products (α particles produced by D-T reactions, tritons and ^{3}He produced by D-D reactions). An important fact to note is that in all these high performance pulses, the thermal-thermal reactions contribute ~ 50% to 60% of the maximum total instantaneous neutron emission rate. This thermal-thermal fraction is confirmed independently using neutron energy spectra measurements [8] which are shown on Fig. 1b).

In Section 2 of this paper, the particle transport aspects of these experiments are addressed. The different mixing models used by TRANSP to determine the tritium and deuterium density profiles and their theoretical implications are discussed. Then the experiments with injection of a 1% mixture of tritium in one deuterium neutral beam source are described. In one of these experiments, after

the tritium source was switched off, the decay of the thermal tritium density was observed and conclusions on the relative diffusion of deuterium and tritium are obtained. This subject has been presented previously [9] but this paper gives a more comprehensive description of the analysis.

Section 3 of this paper deals with the energy transport and the evolution of the energy confinement of these discharges is presented. The discharges which achieve a high neutron emission rate show a period of strongly enhanced confinement. However, the good confinement is only maintained for a short time, and then the ion temperature falls causing a dramatic drop in the thermal-thermal component of the neutron emission rate. The reasons for the good confinement phase and its degradation are discussed.

For the discharge with a high concentration of tritium, it has been suggested that α-particle driven instabilities could affect the energy confinement. The α-particle statistics for the tritium discharge, pulse no. 26148, are given in Section 4 and a comparison is made with the instability threshold for the α-particle driven TAE modes.

Finally a summary and conclusions are presented in Section 5.

2. PARTICLE TRANSPORT

One objective of the first tritium experiments was to determine the characteristics of the particle transport of the thermalised tritium and deuterium and to derive the particle diffusivities of each species. To achieve this aim, the TRANSP simulations were performed assuming different mixing models which determine the tritium and deuterium density profiles. The different mixing models used by TRANSP are described in Section 2.2. Once the tritium density profile is known, the D-D and D-T neutron emission profiles and total emission rates from the beam-beam, beam-thermal and thermal-thermal components are computed in the code using the nuclear fusion cross section fits reported by Bosch[10]. Finally the validity of each mixing model is assessed by comparing the simulations with both the measured D-D and D-T neutron emission rates.

The measurements of the 2.5 MeV (D-D reaction) and 14 MeV (D-T reaction) neutron emission rates are provided by the JET neutron emission profile monitor coupled with fission chambers and silicon diodes for normalisation. A

detailed study of the measurements obtained using these diagnostics is the subject of a companion paper [11]. In the deuterium-tritium discharges with 100% tritium in two neutral beam sources, the high fluxes of 14 MeV neutrons inhibited the measurements of the lower fluxes of 2.5 MeV neutrons. Therefore the different mixing models cannot be distinguished in such discharges. In discharges with a 1% mixture of tritium in one or two of the neutral beam sources, both the D-D and D-T neutron emission rates could be measured and comparisons with the TRANSP simulations are therefore possible.

2.1 Particle balance and mixing models in the TRANSP simulation

The particle balance in TRANSP is computed using measured data for the profiles of effective ionic charge Z_{eff} and the electron density n_e. Z_{eff} is obtained from charge exchange recombination spectroscopy and n_e from interferometer measurements. Quasi-neutrality is then used to determine the impurity density and the total hydrogenic ion density profiles. The thermal hydrogenic ion density profile n_i can then be obtained as the fast ion density from beam deposition is known from the code calculations.

The particle source which is the sum of the thermalised beam ions and the background ions recycled from the wall is also calculated in the simulation. The thermalisation of the beam ions is modelled by a Monte-Carlo technique which takes into account fast ion Coulomb collisions, charge-exchange redistribution and loss, and unconfined orbit losses. The number of ions recycled from the wall depends on the edge particle confinement time which is determined by the H_α diagnostic and the energy of the recycled particles (here the value of the ion temperature near the edge is used). Furthermore, in the case of a multispecies discharge (i.e. D and T), it is possible to control the species fraction of the recycled neutrals. Unless stated, the standard model has been used in which each recycled ion is returned to the plasma as a neutral of the same species. This model was found to be the most appropriate to this set of experiments; this is discussed further in Section 2.5.

Three different mixing models have been used to predict the local evolution of the thermal deuterium and tritium densities in the plasma. The models are termed "constant fraction", "constant velocity", and "proportional diffusivities" to reflect the different ways the separate flows of each of the two

hydrogenic species are prescribed. The models are defined in detail below, where the physical significance of each model is briefly discussed.

2.1.1 *"Constant fraction" model*

In this model no particle diffusion equation is solved. The radial flux of tritium is assumed to be such that C_T the proportion of tritium in the plasma, relative to the thermal hydrogenic ion density n_I, does not vary with radial position. C_T is only a function of time, and depends on the fuelling rates of tritium and deuterium. Therefore the deuterium density n_D and the tritium density n_T have the same profile shape and are given by:

$$n_T = C_T \cdot n_I \text{ and } n_D = (1 - C_T) n_I$$

Similar profile shapes for both species could be produced by an instability driven by the differential gradients of n_D and n_T such that $\nabla n_D / n_D = \nabla n_T / n_T$. The "constant fraction" model implies complete and instantaneous mixing of the two species and may therefore be regarded as the least physical of the three models under consideration.

2.1.2 *"Constant velocity" model*

In this model the radial flow velocities of the tritium and deuterium are assumed to be identical and given by $v_r = \Gamma_I / n_I$. The thermal hydrogenic ion density n_I is obtained as described previously and Γ_I, the total thermal hydrogenic flux, comes from the particle balance equation for n_I. The assumption implies that

$$\frac{\Gamma_T}{n_T} = \frac{\Gamma_D}{n_D} = \frac{\Gamma_I}{n_I}$$

Only the diffusion equation for the species having the lowest volume-averaged density (tritium for this series of pulses) is solved.

$$\frac{dn_T}{dt} = S_T - \nabla.\Gamma_T$$

From the above assumption $\Gamma_T = v_r n_T$ and the particle source of tritium S_T is calculated as described in Section 2.2. The deuterium density is obtained simply by subtraction $n_D = n_I - n_T$.

We consider two illustrative physical examples in which a "constant velocity" model would apply:

Case i) The common, non-diffusive driving forces dominate the hydrogenic particle transport.

The fluxes of D and T may be written as:

$$\Gamma_D \approx n_D \sum_j L_{D,j} F_j$$

$$\Gamma_T \approx n_T \sum_j L_{T,j} F_j$$

according to the general coupled transport matrix equation describing related flows of particles, heat etc. for each species. The driving forces F_j would for example include a temperature gradient term $\nabla T_i/T_i$ [12], whilst diffusion-driving terms $\nabla n_D/n_D$, $\nabla n_T/n_T$ are omitted under the present assumption. Therefore, a constant velocity condition $\Gamma_D/n_D = \Gamma_T/n_T$ would be satisfied for equal off-diagonal transport coefficients $L_{D,j} = L_{T,j}$ of each species in this case.

A "proportional velocities" model would be a more general description to take account of the different isotopic masses of T and D. In this context, it would appear reasonable to assume that $v_T/v_D < 1$. However, this condition could be discounted according to the results of the simulations (see Section 2.4).

Case (ii) Coupled flows of the deuterium and tritium components.

A "constant velocity" model would also apply in the situation of coupling between the radial flows e.g. by friction between parallel flows along stochastic magnetic lines of force. A differential flow velocity would then give rise to a mutual force, eventually dominating other driving forces for the trace species. For strong coupling, the flow velocity of the trace tritium would be maintained close to the deuterium flow velocity, independently of the magnitude of e.g. ∇n_T or other driving forces.

2.1.3 *"Proportional diffusivities" model*

In this model a diffusion equation is solved for each species. The flows of tritium and deuterium are postulated to be mutually independent and are modelled by the sum of two terms, a diffusive and a non diffusive component.

$$\Gamma_D = -D_D \nabla n_D + v_D \cdot n_D$$
$$\Gamma_T = -D_T \nabla n_T + v_T \cdot n_T$$

The solution of the particle balance using available data puts a constraint on the radial flux which is not usually modelled by a diffusion term alone. In this model the particle diffusivities D_D and D_T are chosen arbitrarily; they have the same profile shape and are given as input to the code. A non-diffusive velocity must then be computed for each species, so that the sum $\Gamma_D + \Gamma_T$ satisfies the constraints imposed by the Z_{eff} data and the quasi-neutrality equation. However this still leaves one degree of freedom so one species may be made more "mobile" than the other in order to carry a larger fraction of the total flux. Thus the ratio v_T/v_D is also given as input to the code. In all the simulations using this model $D_T/D_D = v_T/v_D$ = constant is assumed. This constant is adjusted to give the best simulation of the experimental data. It is important to note that the relative contribution of diffusion and convection to the particle flux is not unique and varies with the particle diffusivity profile given as input. However the effective tritium and deuterium diffusion coefficients are uniquely defined by

$$\Gamma_D = -D_D^{eff} \nabla n_D \; ; \; \Gamma_T = -D_T^{eff} \nabla n_T$$

The model does not necessarily result in a ratio D_T^{eff}/D_D^{eff} = constant.

2.1.4 *Discussion*

The three mixing models described above were all used in the TRANSP simulations of the D-T fusion yield in order to allow for the degree of uncertainty in the transport behaviour of the thermalised tritium relative to the deuterium. Indeed, the "constant velocity" and "constant fraction" models each represent opposite extremes of possible particle mixing behaviour under the particular conditions of deuterium flow and deuterium density profile shape present. For a peaked deuterium density profile and

strong outflow, under the "constant velocity" model, a tritium radial outflow exists even in the absence of a tritium density gradient, while in the "constant fraction" model a peaked tritium profile is maintained without any flow even after a central tritium source is terminated.

Conversely for a flat deuterium density profile and low outflow the "constant fraction" model predicts a flat tritium density even with central tritium fuelling, while the "constant velocity" model now maintains a peaked tritium density profile after termination of the central tritium fuelling.

If the shapes of the deuterium and tritium source rates are similar, the tritium and deuterium flows are proportional:

$$\frac{\Gamma_T}{\Gamma_D} = \text{constant} = \frac{D_T^{eff}}{D_D^{eff}} \cdot \frac{\nabla n_T}{\nabla n_D}$$

Hence in this case, if the "proportional diffusivities" model with $D_T/D_D = v_T/v_D$ = constant results in D_T^{eff}/D_D^{eff} = constant, it is identical to the "constant fraction" model. Therefore in such a case the two models result in similar tritium and deuterium density profiles. The two models may be distinguished if the deuterium and tritium source rates differ in shape, e.g. in a discharge with neutral beam injection of deuterium and gas puffing of tritium.

2.2 Simulation of 1% tritium experiment

Pulse no. 26106 was a deuterium - tritium hot ion H-mode discharge in which a small amount of tritium was injected. The main characteristics of this pulse are shown in Fig. 2: approximately 13 kW of tritium is injected for 3s during the high neutron emission phase. In this pulse, both the D-D and D-T instantaneous neutron emission rates could be separately measured. The three models described above have all been used in simulations to predict values for the neutron rates which can then be compared with measured values to determine the transport behaviour of the thermalised tritium ions.

Fig. 3 shows the deuterium and tritium density profiles obtained with the three different mixing models: the calculated deuterium profiles are essentially independent of the mixing model used and the tritium density

profile is only slightly more peaked if the "constant velocity" model is applied. Therefore, all models give equally good fits to both the D-D and D-T observed neutron rates as can be seen in Fig. 4. This is not surprising as the injected deuterium and tritium source rates are similarly peaked on axis for such a discharge and consequently the three models give very similar density profiles in the steady-state and hence the models cannot be distinguished. Nevertheless, the good fits shown in Fig. 4 give us confidence in the validity of the experimental data and the TRANSP simulation.

2.3 The tritium decay experiment

From the above, it is clear that an abrupt termination of the tritium neutral beam is necessary so that the decay of the tritium density profile can be studied. This was achieved in pulse no. 26114, a deuterium-tritium discharge with a 1% mixture of tritium in one of the neutral beam sources. The main characteristics of this medium density H–mode pulse are shown in Fig. 5. At 12s, the neutral beam power was increased to ≈ 9MW, and was kept constant for 3s; the higher starting density gave rise to very similar electron and ion temperature profiles ($T_{i,e}(0) \sim 7$ keV). Some 13 kW of 80 kV tritium ions were injected for 1s between 12.5s and 13.5s. After the tritium source was switched off, the discharge was sawtooth free for a further 0.6s and the decay of the thermal tritium density was observed during this period.

As in the previous case, the different mixing models cannot be distinguished by comparison of the simulation with the D-D neutron data since once again all the models give a similar deuterium density profile. However, one of the three mixing models gives a different tritium density profile in the decay phase. After the tritium beam is switched off, the "constant velocity" model results in a much more peaked profile than the others (see Fig. 6). In this model the flow velocity of tritium is determined by the flow of the dominant deuterium species which is low in the plasma centre. The tritium density is initially peaked due to central beam fuelling and as discussed previously in Section 2.1.4 this model predicts that it remains peaked throughout the decay phase. The other models predict that the profiles will be much less peaked.

Different tritium density profiles give dissimilar neutron emission profiles. This is shown in Fig. 7[a)] where the measured and simulated D-T line integrated neutron emission rates of the horizontal and vertical cameras are

plotted. The "constant velocity" model as well as the "proportional diffusivities" models with $D_T/D_D = v_T/v_D = {}^1/_2$ or 2 do not simulate the measurement. A "proportional diffusivities" model with $D_T/D_D = v_T/v_D = 1$ reproduces well the 14 MeV and 2.5 MeV neutron emission rate. With this model the effective tritium and deuterium diffusion coefficients are roughly equal and, as the tritium and deuterium flows are proportional, this implies that the "constant fraction" model gives very similar results as discussed in section 2.1.4 and shown in Fig. 7. Fig. 7b) shows a comparison between the time evolution of the measured 14 MeV neutron emission rate and simulations with various mixing models confirming that the "proportional diffusivities" model with $D_T/D_D = v_T/v_D = 1$ gives the best agreement with the data. However, the effect of wall recycling (see Section 2.5) is significant if the "proportional diffusivities" model is used, leading to a ratio D_T^{eff}/D_D^{eff} which could vary between 0.5 and 1.0. A weak mass dependence on the diffusion coefficients could therefore not be ruled out.

The ratio of the tritium density to the deuterium density n_T/n_D was found to be more or less constant in radius and decays with an exponential time of 1s. These results are confirmed by a complementary analysis [11].

The effective tritium diffusivity D_T^{eff} is shown in Fig. 8. It is similar to the effective deuterium diffusivity observed in similar pure deuterium discharges and to the effective helium diffusivity observed during helium injection into a deuterium plasma [13]. D_T^{eff} is low in the plasma centre ($D_T^{eff} \approx 0.25\ m^2/s$) and increases sharply towards the edge to $\sim 2\ m^2/s$.

In summary, the "constant velocity" model and a "proportional velocities" model with $v_T/v_D < 1$, which would imply an even more peaked tritium density profile, can clearly be excluded. The other two models however give equally good fits to the data because this experiment is one of the special cases discussed in Section 2.1. In the TRANSP simulations described in the remainder of the paper the "proportional diffusivities" model with $D_T/D_D = v_T/v_D = 1$ is therefore used unless otherwise specified.

2.4 The high fusion power discharge

The good agreement reported in the previous sections between the measured and simulated neutron data confirmed the validity of the TRANSP

simulation. The code was therefore used to choose the on/off times of the tritium sources to optimise the performance of discharges with injection of 100% tritium. Two discharges with two of the neutral beam sources fuelled with pure tritium were performed. The main characteristics of the best discharge, pulse no. 26148, were reported in [4]. For the same reasons as discussed in Section 2.2, the D-T neutron emission data are well reproduced by TRANSP regardless of the particle mixing model used. An example of such a good agreement is shown in Fig. 9 where the time evolution of the simulated line-integral neutron emission rates from a central (#16) and an outer (#18) channel of the neutron profile monitor are compared with the experimental values. There are interesting features to note from this Figure:

i) The effect of the sawtooth crash at 12.37s is very clearly seen in the signal from the central channel which decreases by a factor 2. This sharp decrease is due to the collapse of the beam-plasma contribution which is dominant in the early stage of these discharges. The redistribution of the fast ions from the plasma centre to the outer region is simulated using a sawtooth model based on the Kadomtsev description [14]. The predicted increase of neutrons near the edge after the sawtooth crash is detected by the outer channel as seen in Fig. 9c).

ii) After the sawtooth crash, the signal of the central channel recovers as the centre of the plasma is re-fuelled by the neutral beam. However, at t = 12.7s, the rate of increase of the central channel signal decreases corresponding to a change in the evolution of the central ion temperature which starts to saturate. Nevertheless, the outer channels still increase after that time due to a broadening of the ion temperature which explains why no change of slope is seen in the evolution of the total neutron emission rate.

2.5 Effect of wall recycling

As mentioned in Section 2.1, it is possible to vary the species fractions of recycling neutrals in the TRANSP code. The effect of wall recycling on the deuterium and tritium density has been investigated for the different discharges presented in the previous sections. Different recycling scenarios have been assessed using the different mixing models:

a) All hydrogenic ions striking the walls are recycled as deuterium. This may be thought to be the more likely scenario since JET had not previously used tritium and the walls were almost completely loaded with deuterium.

b) The particles are recycled unchanged.

c) 20% of all hydrogenic ions striking the wall are recycled as tritium. This scenario has only been considered for pulse no. 26148 as this pulse was the second of the two tritium shots.

In the case of the "constant fraction" model, the ratio n_T/n_D only depends on the source of thermal ions from the beam and remains the same regardless of the recycling scenario considered. The code adjusts the particle confinement time of the minority ions τ_T (i.e. tritium) near the edge to be consistent with the chosen scenario. In case a), τ_T near the edge is set to be longer than the duration of the high neutron rate phase and therefore no change in the tritium density (and consequently in the D-T neutron yield) is observed.

In the case of the "constant velocity" model, the tritium density profile shape is determined by the flow of the dominant deuterium species which hardly changes with the different recycling scenarios considered here. The main difference between the three recycling scenarios is observed near the edge where the tritium density is much lower in case a) than in case b) or c). However the central tritium density is only slightly lower in case a). Therefore the D-T neutron emission rate is only slightly lower in case a) and the conclusions on this model presented in Section 2.3 remain unaffected by the wall recycling.

For all the deuterium-tritium pulses the choice of recycling scenario produces clear differences in the simulation of the D-T neutron yield only if the "proportional diffusivities" model is used: this can be seen in Fig. 10 for pulse no. 26148. If it is assumed that the walls are so heavily loaded with deuterium that only deuterium is recycled then the simulated 14 MeV neutron emission rate is half the measured value. A 20% probability of returning tritium regardless of the species of the incident particle leads to a neutron emission rate which is too high. The outflow of tritium can now respond to changes in the edge ∇n_T brought about by changing the recycling conditions. The D-T

neutron data are only accurately reproduced if it is assumed that each recycling ion is returned to the plasma as a neutral of the same species. These results imply that the isotope ratio in the plasma and the wall quickly reach equilibrium.

3. ENERGY TRANSPORT

The series of pulses which included the first tritium experiment generally had very good confinement. However the enhanced performance phase was only maintained for a short time (~ 1 sec) before the ion temperature decreased causing a dramatic drop in the thermal-thermal component of the neutron yield. This degradation of performance did not at first appear clearly to follow the same pattern in each discharge and a careful analysis has been completed which gives a better understanding of the sequence of events. This section gives a more comprehensive analysis than previously [15] and investigates the behaviour of the best deuterium discharge no. 26087 in particular. Possible reasons for the formation of the enhanced confinement phase and its subsequent loss are discussed. Finally, there is a brief comparison between the behaviour of pulse no. 26087 and other pulses in the series.

3.1 Time evolution of the thermal confinement

The performance of four of the discharges has been followed throughout the duration of the pulse. All the discharges have similar plasma parameters and neutral beam heating power - see Table I, but do not all exhibit the same confinement behaviour.

Figures quoted in Table I for the value of line averaged effective charge $\overline{Z}_{eff}$ and the central value of the ion temperature $\hat{T}_i$ relate to data used in the present TRANSP calculations and differ slightly from those quoted previously [4]. Since the initial publication of results from these experiments, values of Z_{eff} from charge exchange recombination spectroscopy have been recalculated using revised values of neutral beam injection data. The present TRANSP calculations use a radial profile for Z_{eff} rather than a fixed value given by visible bremsstrahlung measurements which was used previously. All values for $\overline{Z}_{eff}$ and $\hat{T}_i$ given in Table I are within the experimental errors quoted in [16] which gives details of the measurements obtained by charge exchange recombination spectroscopy for this series of pulses. Electron

density data from interferometry has also been reprocessed since the earlier publication [4].

Fig. 11 shows the different evolution of the thermal confinement time τ_{TH} for these pulses compared to the value predicted by the H-mode scaling expression ITERH92-P [17]. A D_α emission signal is also plotted which shows the L-H transition and the occurrence of edge localised modes (ELMs). The thermal confinement time is calculated using the measured diamagnetic energy W_{dia} and the TRANSP calculation (every 25 ms) of the perpendicular fast ion energy $W_{\perp\,fast}$. The measured W_{dia} is used because the simulated values do not fit exactly the time evolution of the measurements (see Fig. 1a)).

$$\tau_{TH} = \frac{W_{th}}{P_{tot} - \dot{W}_{th}}$$

$$P_{tot} = P_i + P_e + P_{OH} \;\; ; \;\; W_{th} = W_{dia} - \frac{3}{2} W_{\perp fast}$$

The power input terms to ions and electrons, P_i and P_e, and the ohmic power P_{OH} are also calculated by TRANSP. The radiated power in these discharges only represents ~ 10% of the total injected power before the massive impurity influx known as the "carbon bloom" [18, 19, 20] occurs.

The high performance shots nos. 26087, 26095 (a D-T discharge with a small amount of injected tritium) and 26148 (the best D-T discharge) change from L-mode to H-mode and then into a regime having enhanced confinement with values approximately twice the ITERH92-P value and a factor three above the Goldston L-mode scaling expression [21]. (The ITERH92-P expression predicts values slightly higher than those from the DIII-D/JET [22] expression for these pulses). In Fig. 11 the letter M indicates the times of the maximum measured total neutron emission rate. After the collapse of the neutron emission the plasmas do not recover the enhanced confinement, exhibiting normal H-mode confinement. By contrast the discharge no. 25432, with similar neutral beam input power to the previous three but in double-null configuration does not show any enhanced performance and the confinement time follows the value predicted by the ITERH92-P scaling expression throughout the heating phase.

In the pulses showing enhanced performance the confinement appears to decrease shortly before the maximum instantaneous neutron emission rate is achieved. For some pulses however it is impossible to state that the confinement has definitely been lost before the peak rate is reached. This is due to the poor time resolution of the diagnostic data used in the calculation of τ_{TH}. This is the case for pulse nos. 26095 and 26148 in particular. However for pulse no. 26087, which is discussed in more detail in the next section, the good confinement phase is clearly lost prior to the peaking of the neutron emission rate.

3.2 Time evolution of pulse no. 26087

The signal of D_α emission plotted in Fig. 11 shows that in pulse no. 26087 there are ELMs during the early part of the discharge but no ELMs or sawteeth during the period of enhanced confinement. This pulse has been analysed in detail in order to try and determine the reasons for the high confinement phase and its deterioration. Fig. 11 shows that the calculated confinement time starts to decrease from 13.23s some 170 ms before the time of the peak neutron rate at 13.4s.

Fig. 12 shows the evolution of several key parameters during the period of high confinement and its subsequent deterioration. Central and edge values of the ion temperature T_i and effective charge Z_{eff} from charge exchange recombination spectroscopy measurements are plotted, the data points being marked at 50 ms intervals by symbols. Throughout the high confinement phase the ion temperature continues to increase. At about 13.2s the confinement starts to decrease followed by a fall in the edge and central T_i values which is accompanied by a drop in the central neutron channel measurement. Fig. 1b) shows that the decrease in total neutron rate is primarily due to a large drop in the thermal-thermal component which is directly proportional to the square of the ion temperature [3] for this range of temperatures. The beam-thermal component only drops later due to the sawtooth crash at $t = 13.47$s. The electron temperature T_e profile measurements by the ECE grating polychromator shown in Fig. 13 also show flattening from the edge from about 13.2s. Fig. 12e) shows the sum of the electron and ion conduction and convection powers reaching the edge of the plasma as calculated by TRANSP. The apparent loss in confinement gives rise to a dramatic increase in the power conducted to the X-point target plates

which in turn results in a large increase in the measured C-III light emission from the edge, the so-called "carbon bloom" and a large increase in the measured edge and central values of Z_{eff}. It should be noted however that the measured electron density continues to rise at the edge of the plasma and the measured particle confinement time is also increasing during this period.

Although a good simulation of the pulse was obtained with TRANSP as shown by the agreement between the measured and simulated neutron yield in Fig. 1[b)] the time resolution of the estimated quantities could not be better than 50 ms since differentials are being calculated, but despite these uncertainties there is at least 70 ms between the loss of confinement and the roll-over of the neutron yield for this pulse.

In summary the degradation in performance from 13.2s onwards as shown by the calculated thermal confinement time is reflected in the measured temperature profiles which flatten from that time causing the neutron yield to fall. As the power being deposited on the limiter builds up, the impurity level increases, finally leading to the "carbon bloom".

3.3 Results of transport analysis

From the calculated ion and electron power balances it can be seen that more than 85% of the input power goes through the ion channel and therefore the uncertainty in the electron conduction is large. Thus an accurate ion power balance can be obtained but the electron power balance is uncertain. The discussion will therefore be confined to the ion power balance. From this power balance (Fig. 14) it can be seen that the main loss is ion heat conduction and convection only becomes important near the edge. The pulse has good central confinement ($\chi_i \approx 0.3$ m^2/s) during the enhanced confinement phase as shown in Fig. 15 and χ_i is only a factor 3 to 4 above neoclassical. The edge value ($\chi_i \sim 2$ m^2/s) is lower than that of a conventional H-mode. During the normal H-mode phase the conductivity is higher across the whole radius. Fig. 16 shows χ_i at normalised radii $\rho = 0.3$ and 0.7, the symbols indicating the times of the calculation. The edge conductivity starts to rise soon after 13.1s closely followed by the central value. After the "carbon bloom" the conductivity remains at a higher level across the whole radius. This is in marked contrast to the behaviour of the particle diffusivity where the edge values do not change until shortly before the sawtooth at around 13.4s and

the central diffusivity regains its low value after the collapse. A profile of the thermal confinement time can be obtained from the local TRANSP calculated values of W_{th}, P_i, P_e and P_{OH}. Fig. 17 shows the edge confinement time decreasing steadily from ~ 13.2s onwards. The confinement at the centre starts to decrease at the same time but there is a pause around 13.25s before the central confinement is finally lost. These results tend to indicate that the energy confinement is being lost at the edge first but with the ± 50 ms time resolution of these calculations a conclusive statement cannot be made.

An effective ion diffusivity D_i^{eff} which does not take into account any particle pinch can be defined by:

$$\Gamma_i = - D_i^{eff} \cdot \nabla n_i$$

where Γ_i is the total ion particle flux and n_i is the total ion density including the fast ions. The effective ion diffusivity for the best deuterium discharge, pulse no. 26087, is shown in Fig. 18 at different times. During the high performance phase (t = 13.15s), the diffusivity profile is more or less flat across the whole radius and has a very low central value ($D_i^{eff} \sim 0.25$ m^2/s) but increases sharply near the edge for normalised radius $\rho \geq 0.8$. It is interesting to note that the central value increases steadily after 13.15s, but the edge value does not rise. There is a marked increase at all radii just before the sawtooth crash (t = 13.47s). At a time after the sawtooth crash (t = 13.7s), the total neutron emission rate is already half of its maximum value (see Fig. 1[b]) and the diffusivity profile changes its shape. It is more hollow with edge values twice those in the previous phase but the central diffusivity has reverted to its previous low value. The plasma does not recover the good edge particle confinement shown at the time of maximum neutron yield.

In summary, the particle confinement shows an enhanced phase, corresponding to the high fusion part of the discharge. There is a gradual central degradation before the good confinement is definitely lost after the "carbon bloom" occurs. These features are observed in all the hot ion H-mode discharges performed during the series regardless of the presence or absence of tritium.

3.4 Possible explanations for confinement behaviour

3.4.1 MHD activity

Fig. 19 shows the time evolution of the amplitude of the n = 1 MHD activity together with the thermal confinement time for pulse nos. 26087, 26095 and 26148. Comparison with the value predicted by the ITERH92-P scaling expression shows the period of enhanced performance. Fast MHD data indicates that the most prominent activity is fishbone bursts [23]. In pulse no. 26087 the MHD activity is low throughout the ELMing phase around 12.6s but is increasing steadily by 13.2s when the confinement is starting to degrade. At 13.47s there is a sawtooth crash. Although the degradation in confinement appears to coincide with an increase in MHD activity in this discharge this is not the case for pulse nos. 26095 and 26148, as discussed in Section 3.5.1.

Fig. 20 shows the time evolution of the ratio of β as calculated by TRANSP to the Troyon beta limit [24] for pulse nos. 26087, 26095 and 26148. For pulse no. 26087 β increases steadily until about 13.25s where the slope of the ratio changes before finally rolling over at a value of 0.75. It is clear from Fig. 20 that although β has not reached the Troyon beta limit it is being checked by some mechanism. A full stability analysis to estimate the Troyon beta limit for this particular discharge is at present being prepared.

3.4.2 Degradation in beam heating of the plasma

One obvious reason for the saturation of T_i could be that the neutral beams are prevented from heating the centre of the plasma due to the increasing density. Fig. 21[a)] shows the input power, versus time, along with the central density in Fig. 21[b)]. Fig. 21[c)] shows the reduction in the fast particle source rate at the plasma centre due to the poorer penetration with increased density. However from Fig. 21[d)] we see that the heating power to the central third of the plasma continues to increase slightly because the energy transferred from the fast ions is increasing with density. Hence the TRANSP calculation does not indicate that the temperature saturation is connected with any degradation in the fast ion heating.

3.4.3 *The stabilisation of ion temperature gradient instability by the peaked density profile*

Fig. 22 shows the time evolution of the ion thermal conductivity χ_i, the density scale length $L_{ne} = - n_e/\nabla n_e$, and $\eta_{ie} = L_{ne}/L_{Ti}$ at $\rho = 0.3$ for pulse no. 26087. The density profile becomes more peaked until 13.25s when the profile flattens and the density scale length starts to rise. The value of χ_i begins to increase at $\rho = 0.3$ at around this time. The value of η_{ie} is above 5 throughout this period and decreases to a minimum at about 13.25s. At 13.4s there is a large increase in η_{ie} at the same time as χ_i increases more steeply; η_{crit} according to Romanelli et al [25] is about 5 at this time. Although there is some correlation between the deterioration of the confinement and increasing η_{ie}, in the early part of the discharge when the confinement is good ($t \sim 13.1s$) η_{ie} is also quite large. L_{ni} calculated from the TRANSP estimate of the ion density n_i follows the same time evolution as L_{ne} but is higher throughout. Hence η_i is always greater than η_{ie} and even further from the critical value.

3.4.4 *Stabilisation due to current profile changes*

All the high performance pulses exhibit some of the same characteristics found in the DIII-D VH-mode [26]: particularly steep edge gradients and a large edge bootstrap current as shown in Fig. 23 for pulse no. 26087 at 13.2s. The fact that the predicted value of the bootstrap current density is larger than the total current density at the edge is confirmed by the measurement of a negative loop voltage. The large bootstrap current, 0.8 MA in a total plasma current of 3.1 MA, is further confirmed by an equilibrium reconstruction performed by the EFITJ [27] equilibrium code which also allows a finite edge current.

Fig. 24 shows the time evolution of ℓ_i as calculated by TRANSP for the three pulses with enhanced thermal confinement times. In pulse no. 26087, as the plasma moves into the enhanced phase soon after 12.6s, ℓ_i starts to drop more steeply indicating increased broadening of the total current profile. Between 13.1s and 13.2s when the bootstrap current reaches its maximum value ℓi starts to increase showing that the total current profile is starting to peak. This is the time when the enhanced confinement is beginning to disappear and χ_i starting to rise.

The existence of steep edge pressure gradients and significant edge current points to a consideration of ballooning stability. The ideal ballooning equation [28] depends on two dimensionless parameters $\alpha \propto p'$ where p' is the pressure gradient and $\Lambda \propto < j \cdot \underline{B}/B^2 >$ where j is the current density and B the total magnetic field. Usually the ballooning equation is solved as an eigenvalue equation for α with Λ given. Across the bulk of the plasma there exist two marginally stable values of α. These define an unstable zone which separates the first (small α) stable region from the second (large α) stable region. Close to the edge, however, the first and second regions can coalesce and the unstable region disappears when Λ exceeds a critical value Λ_{crit}. The plasma in this region is then stable to ballooning modes at all values of the pressure gradient.

A time-dependent marginal stability ballooning calculation has been performed for some of the high performance discharges. The results show that pulse no. 26087 has access to and enters the second stable region over a small area near the plasma edge during the enhanced performance phase of the discharge. At the termination of this phase the connection region is closed and the plasma becomes ballooning unstable. The pressure gradient profile is obtained from the reflectometer electron edge density and ECE electron temperature, assuming the total pressure p is twice the electron pressure p_e. The current density at the edge is obtained from a simple calculation of the bootstrap current.

In Fig. 25[a] the parameter Λ for pulse no. 26087 is plotted as a function of time for a particular surface close to the edge of the plasma. The critical value Λ_{crit} for coalescence to occur is plotted together with the experimental value Λ_{exp}. Superimposed is the thermal confinement time τ_{TH}. During the enhanced phase of the discharge $\Lambda_{exp} > \Lambda_{crit}$ giving access to the second stable region, but soon after the time of the peak neutron emission rate at t = 13.4s $\Lambda_{exp} < \Lambda_{crit}$ implying that access is lost. This is seen more graphically in Fig. 25[b] where the marginally stable boundaries for the same flux surface close to the edge are plotted together with α calculated from experimental data showing that for the VH-phase of the discharge the pressure gradients are in the second stable region. During the ELMing period the more accurate reflectometer data is not available so that the estimate of α during the ELMs is questionable. The experimental pressure gradients are seen to decrease at the

time τ_{TH} starts to drop. However access to the ideal second stability region is maintained.

Fig. 12[h)] shows that the impurity level and hence the resistivity near the edge starts to increase very gradually from about 13.2s. The inclusion of the effects due to resistivity in the ballooning instability have not yet been performed but model calculations indicate that access to the stable region may be more restricted than shown in Fig. 25[b)].

3.5 Comparison of pulse no. 26087 with pulses no. 26095, 26148 and 25432

3.5.1 High performance pulses no. 26095 and no. 26148

As shown in Fig. 11 both these pulses have values of the thermal confinement τ_{TH} which are considerably higher than those predicted by the ITERH92-P scaling expression although neither attains quite the level of performance of pulse no. 26087. The loss of good confinement happens much more rapidly in these pulses and due to the lack of resolution in the data it is not possible to state that this definitely occurs before the collapse of the neutron emission. Neither of the pulses regains good performance after the collapse.

In the 1% T pulse no. 26095 the thermal conductivity χ_i was also very low in the centre ($\chi_i \sim 0.3\ m^2/s$) during the enhanced phase which was maintained for as long as 1s. Although the amount of neutral beam power was slightly lower than for pulse no. 26087 higher values of T_e and T_i were reached - see Table I. In this pulse the loss of good confinement seems to occur more rapidly. Profile values of T_i and Z_{eff} did not change and χ_i did not rise until about 13.65s, about 100 ms before the time of maximum neutron yield at 13.76s. As the level of heat flow to the edge did not start increasing until late in the discharge, less power reached the X-point target plate. In this pulse one of the neutral beams failed just before the time of collapse in the neutron emission rate. TRANSP calculations show some indication of a loss of beam heating to the centre of the plasma during this period which may be a contributory factor to the subsequent collapse. Fig. 19 shows that during the ELMing phase around 12.7s the n = 1 MHD activity rises until a sawtooth occurs. After this the activity remains low and the good confinement lasts for

longer than in pulse no. 26087. There is no sign of the activity increasing when the confinement starts to degrade.

The best D-T pulse no. 26148 had a lower volume averaged electron density and reached somewhat lower temperatures - see Table 1. The discharge also had a higher level of impurities, during the enhanced phase Z_{eff} is 30% higher across the whole profile compared to that for pulse no. 26087 at a comparable time. The thermal conductivity is higher, about 0.5 m^2/s in the centre, and the good confinement is only maintained for about 0.5s. The particle diffusivity D_i^{eff} is also higher than for pulse no. 26087. Once again the good performance is maintained until just before the time of peak neutron emission rate at 13.28s. There is little change in the Z_{eff} profile until 13.2s but T_i at the edge is rising until that time. The calculated power to the edge started to rise from 13.15s and reaches 20 MW. Fig. 19 shows that fishbone activity is rising steadily throughout the period of good confinement, but does not appear to correlate with the decrease in the thermal confinement time. Finally, the discharge is terminated by a sawtooth at 13.3s followed by ELMs. Fig. 20 shows that the ratio of β/β_{TROYON} increases steadily until the time of the sawtooth when it suddenly falls. There is no indication that the discharge has reached a limiting value of β before this time.

There is no obvious correlation for these two pulses between the evolution of the density scale length L_{nc} or η_{ic} and the thermal conductivity. Fig. 24 shows the same sort of time evolution of ℓ_i for these two pulses as for pulse no. 26087. There is an increased broadening of the current profile as the plasma enters the enhanced regime but in these pulses it is not so evident that the current profile starts to peak before the time of maximum neutron emission as indicated by the letter M. Ballooning stability calculations show that pulse no. 26095 enters the second stable region over a relatively large area near the plasma edge. The electron density data at the edge is not so reliable for pulse no. 26148 but calculations show that access to the second stable region is certainly possible.

3.5.2 *Double-null H-mode pulse no. 25432*

Fig. 11 shows that pulse no. 25432 does not have a phase with an enhanced thermal confinement time even though the plasma parameters are

comparable to those in pulse no. 26087 and the neutral beam input power is even higher - see Table I.

TRANSP calculations show that the neutral beam heating of the plasma is much less efficient for pulse no. 25432 than for pulse no. 26087. In the former discharge at 10s when 8 MW of 140 kV/D beam heating was switched on the peak density ($\sim 2 \times 10^{19}$ m^{-3}) was relatively low and calculations show that about 40% of the input power is lost by shine through. This loss is still large for some time after the remaining 8 MW is switched on at 11s. In contrast, in pulse no. 26087 when the initial 4 MW of 140 kV/D beams was switched on the peak density was higher ($\sim 2.5 \times 10^{19}$ m^{-3}) and less than 25% of input power is lost. Calculations of the beam heating profiles for both pulses show that particularly at earlier times the heating to the ions is much greater for pulse no. 26087. This additional heating leads to much larger values for T_i particularly near the edge of the plasma. Fig. 26 shows the measured ion temperature profiles for both pulses at times just before the respective peak neutron emission rates. As pulse no. 25432 was in double-null configuration the plasma was slightly more circular with a larger minor radius.

The lower values of T_i over much of the radius in pulse no. 25432 together with a higher central impurity density lead to a lower thermal-thermal neutron emission rate. In contrast to all the pulses showing enhanced performance the total neutron emission rate for this pulse is dominated by the beam-thermal component. This is comparable in value to that for pulse no. 26087 but the thermal-thermal component is only about 25%.

The electron density profile for pulse no. 25432 is broader being lower in the centre and less steep at the edge. Electron temperature values are also lower particularly at the edge. The calculated edge bootstrap current is therefore lower than in pulse no. 26087 and ℓ_i continues to increase throughout the pulse. Ballooning stability calculations show that the dimensionless parameter Λ does not reach the level of Λ_{crit} and there is therefore no access to the second stability region at the edge for this pulse.

4. THE α-PARTICLE STATISTICS FOR THE D-T PULSE NO. 26148

The Monte Carlo techniques used to model the fast ions from neutral beam injection have been extended to model the fast fusion products from the D-D

reaction (i.e. tritons and ^{3}He) and the D-T reaction (i.e. α-particles). Finite orbit effects are taken into account in the computation of their slowing down and heating of the thermal plasma. The α-particle statistics from the simulation of the D-T discharge, pulse no. 26148, are listed in Table II at a time close to the maximum neutron yield. Values quoted in Table II for the power transferred from the α-particles to the ions and electrons are lower than those quoted previously [4] where the results were obtained from an instantaneous equilibration model. The present TRANSP calculations use a radial profile for Z_{eff} rather than a fixed value; this results in heating profiles which are more peaked than in [4] but this only has a slight effect on the total heating power. The uncertainties in the Z_{eff} profile [16] could lead to an error in the central heating power of as much as 20%. Most of the α heating goes to the electrons, the α heating of ions being one order of magnitude lower. The orbit loss of α-particle power to the limiter and walls represented only ~ 6% of the total α heating. Furthermore, the total α heating was overshadowed by the neutral beam heating; hence one would not expect any observable effect of the α-particles on the electron temperature, and none was seen.

The normalised profiles of the α-particle density n_α, the toroidal α-particle beta β_α, the total α-particle heating rate P_α, the electron density n_e and the fast (tritium + deuterium density n_{fast} are compared in Fig. 27. All α-particle related profile shapes are much more peaked than the electron or the neutral beam density; the steepest gradients occur for a normalised radius $\rho < 0.3$.

The deuterium-tritium pulse no. 26148 offered the opportunity to observe, possibly, the stimulation of collective α instabilities such as the toroidicity induced Alfvén eigenmodes (TAE) [29]. In toroidal geometry Alfvén modes are not strongly damped at all frequencies as they are in cylindrical geometry. Toroidicity induced gaps occur in the continuous spectra at certain frequencies and a discrete Alfvén mode exists inside these gaps. If for a given toroidal mode number n, safety factor q(r) and Alfvén velocity $C_A(r)$, gaps associated with different poloidal mode number m values thread through the plasma column, the corresponding Alfvén gap mode is not subject to continuous damping. A residual damping due to the Landau interaction with thermal electrons and ions, electron collisions, etc., can be offset by the inverse Landau damping with α-particles, resulting in unstable global Alfvén modes. The source of free energy for these modes is related to the α-particle pressure gradient.

Calculations [30] show that Alfvén gap modes with $n > 5$ are very hard to excite in JET plasmas. The gap structures and continuum damping for perturbations with $n = 1$ to 5 have been investigated with the toroidal MHD spectral code CASTOR. From this study, the mode numbers which appear to be most dangerous have been selected.

Marginal stability curves for the selected mode numbers have been obtained with a separate code (based on the approximation used by Betti and Freidberg [31]) which evaluates the α-particle drive and the background electron and ion Landau damping. This analysis shows that the toroidicity-induced Alfvén eigenmode (TAE) with $n = 3$ and dominant $m = 3, 4$ is the most dangerous one for the parameters of discharge no. 26148. The marginal stability boundary for this mode, at the time where the α-particle production reaches its maximum is shown in Fig. 28, where C_{AG} and $\beta_{\alpha G}$ denote the Alfvén speed and the α-particle beta at the gap radius, r_G, where $q_G = (m + 1/2)/n = 7/6$. v_α^{birth} denotes the α-particle birth velocity. The hatched region reflects the sensitivity of the marginal stability curves to uncertainties in the gap radius, the electron and ion temperatures at the gap, the α-particle pressure scale length, $L_{\alpha G} = - (d\ell np_\alpha/dr)^{-1}_G$, etc. The α-particle pressure profile has been evaluated by the TRANSP code. The experimental values of the relevant parameters (with error bars) are indicated in the figure caption. Also shown in the figure is the point corresponding to the values of $\beta_{\alpha G}$ and v_α^{birth}/C_{AG} at the selected time. This point with its error bars lies outside of the unstable domain on its right, corresponding to $v_\alpha/C_{AG} > 1$.

The conclusion from this analysis is that α-particle driven global Alfvén modes were stable in pulse no. 26148. This result is confirmed by ion cyclotron emission measurements (ICE) [32] where no evidence from saturation in the ICE signal caused by anomalous α-particle losses was obtained during the high performance phase. However, the proximity of the relevant parameters to their marginal stability values lead us to believe that the excitation of α-particle driven global Alfvén modes in future JET experiments with a 50:50 DT mixture is a realistic possibility. In particular, the unstable domain may be accessed by operating at lower target plasma densities (i.e. lower v_α/C_{AG}) and higher ion temperatures, so to maintain a significant level of α-particle production.

5. SUMMARY

The TRANSP code has been used extensively to analyse the series of pulses which included the first tritium experiments. Extremely good simulations of various measured quantities, particularly of neutron emission profiles, have given considerable confidence in the internal consistency of the measured data. The code is therefore a powerful tool with which to investigate the behaviour of these discharges. This paper reports on studies of the particle transport of D and T and on possible reasons for the enhanced performance behaviour of these hot ion H-mode plasmas.

The particle transport properties of tritium have been shown to be very similar to those of deuterium and a model in which $\Gamma_T = - D_T^{eff} \nabla n_T$ with $D_T^{eff} \approx D_D^{eff}$ gives a good fit to both the D-D and D-T neutron data. The flows of the two species are therefore mainly driven by their own local density gradients. However a mass dependence on the diffusion coefficients could not be ruled out. The effect of wall recycling on the deuterium and tritium density has been investigated and the isotope ratio in the plasma and the wall has been shown to quickly reach equilibrium.

The hot ion H-mode plasmas which were used in this series of experiments were found to have an enhanced confinement phase in which the energy confinement time is up to twice the values predicted by H-mode scaling expressions. The properties of this high confinement phase are very similar to those of the DIII-D VH-mode. The local analysis shows that the ion thermal conductivity is reduced across the whole profile during the enhanced confinement phase, and that the coefficient of particle diffusivity is similarly reduced.

The reasons for the improved confinement phase are not clear. The stabilisation of the η_i mode due to the peaking of the density gradient has been investigated but seems to be unlikely since although η_i is increasing during the collapse phase it is also quite high during the early part of the discharge. However the entry of the edge into the second ideal ballooning stability region due to the formation of a large edge bootstrap current, does show a clear correlation with the improvement of the confinement in the edge region and hence the generally enhanced performance of the plasma. It is not clear however whether the high edge current density initiates or is a consequence of this enhanced confinement, nor whether shear stabilised modes other than the above are playing a role.

However the analysis described in this paper gives no clear explanation for the degradation in confinement which clearly happens in pulse no. 26087 some time before the final impurity influx. There are indications from the calculated local profiles of the thermal confinement time τ_{TH} and the thermal conductivity χ_ι that the good confinement goes slightly earlier at the edge than in the centre of the plasma. This sequence would appear to be supported by diagnostic measurements of the ion and electron temperatures which show the profiles flattening from the edge. However the plasma edge appears to still have access to the second ideal ballooning region when the confinement starts to degrade.

In pulse no. 26095 the sequence of events at the end of the pulse happens much more rapidly and it is impossible to state that the enhanced confinement is lost significantly before the influx of impurities. There are no indications that confinement is lost initially at the edge of the plasma. In pulse no. 26148 events also occur very rapidly. The discharge is terminated by a sawtooth followed by ELMS and there is no definite indication of loss of confinement or a limit in the rise of β before this time. The termination and the role of the MHD activity in these high-performance discharges are dealt with by other papers in this series [33, 34].

Finally the possible occurrence of toroidicity induced Alfvén eigenmodes (TAE) instabilities during the high fusion power D-T discharge has been investigated. The TAE modes appear to have been stable; a higher β_α would be one of the conditions to stimulate such modes and this may be achieved during the next tritium experiments at JET.

ACKNOWLEDGMENTS

The authors wish to acknowledge the work of their colleagues in the JET team in obtaining these high performance pulses. We also thank D.M. McCune for his work on the TRANSP α-particle Monte-Carlo code and T. Elevant for providing the neutron energy spectra data.

Table I: Main Plasma Parameters for Pulse Nos. 26087, 26095, 26148 and 25432

Parameter	Units	No. 26087	No. 26095	No. 26148	No. 25432
Time	S	13.35	13.70	13.25	12.15
Volume averaged Electron density	$10^{19}m^{-3}$	3.3	3.2	2.4	3.1
Central Electron Temperature	keV	10.5	11.9	9.9	10.0
Central Ion Temperature	keV	18.0	22.0	18.0	16.4
Line Averaged effective charge		1.6	1.9	2.2	1.5
NB Power (P_{NB})	MW	14.9	14.2	14.3	15.6
Elongation at edge		1.65	1.68	1.69	1.50
Minor Radius	m	1.06	1.05	1.05	1.08
Triangularity		0.43	0.43	0.41	0.43

Table II:

α-particle statistics from the TRANSP simulation of pulse no. 26148 at 13.2s

Total power transfers:		
from α–particles to electrons	:	210 kW
from α-particles to ions	:	25 kW
from neutral beam to electrons	:	1.8 MW
from neutral beam to ions	:	9.6 MW
neutral beam loss by shine-through	:	0.5 MW
neutral beam loss by charge-exchange	:	1.4 MW
α-particle loss by orbit losses	:	15 kW
Central power transfers *:		
from α-particles to electrons	:	10.6 kW/m^3
from α-particles to ions	:	1.3 kW/m^3
from neutral beam to electrons	:	69.7 kW/m^3
from neutral beam to ions	:	455 kW/m^3
α-particle concentrations:		
ratio of α-particle to electron central density *	:	5.0×10^{-4}
volume averaged toroidal α-particle beta $< \beta_\alpha >$	:	1.42×10^{-4}
central toroidal α-particle beta $\beta_\alpha(o)$ *	:	8.9×10^{-4}
α-particle birth velocity v_α^{birth}	:	1.3×10^7 m/s
central Alfven velocity $c_A(o)$	:	7.08×10^6 m/s
ratio $v_\alpha^{birth}/c_A(o)$	:	1.84

* Volume averaged over the central 30 cm of the plasma

REFERENCES

[1] Keilhacker, M., and the JET team, Phys. Fluids B2 (6), June 1990.

[2] Goldston, R.J., McCune, D.C., Towner, H.H., et al., J. Comput. Phys. 43 (1981) 61.

[3] Stubberfield, P.M., Balet, B. and Cordey J.G., Plasma Phys. and Control. Fusion 33 (11) (1991) 1255.

[4] The JET team, Nuclear Fusion 32 (1992) 187.

[5] Reichle, R., Clement, S., Gottardi, N., et al., Europhysics Conf. Abstracts (Proc. 18th European Conference on Controlled Fusion and Plasma Physics), EPS, Berlin, Vol. 15C, Part III, (1991) 105.

[6] Andrew, P., Coad, J.P., Ehrenberg, J., et al., "Experiments on the release of tritium from the first wall of JET", Nuclear Fusion, accompanying paper in this issue.

[7] Balet, B., Cordey, J.G., Stubberfield, P.M., Plasma Phys. and Control. Fusion 34 (1) (1992) 3.

[8] Olsson, M., V. Belle, P, Conroy, S., et al., Plasma Phys. and Control Fusion 35 (1) (1993) 179.

[9] Balet, B., Cordey, J.G., Jones, T.T.C., et al., Europhysics Conf. Abstracts (Proc. 19th European Conference on Controlled Fusion and Plasma Physics) EPS, Innsbruck Vol. 16C, part I (1992) 263.

[10] Bosch, H.S., "Review of Data and Formulas for Fusion Cross-sections", IPP I/252, September 1990.

[11] Marcus, F.B., Adams, J.M., Balet, B., et al., "Neutron Emission Profile measurements during the tritium experiments at JET", Nuclear Fusion, accompanying paper in this issue.

[12] Gruber, O., Europhys. Conf. Abstracts. 148 Part II (1990) 841.

[13] Jones, T.T.C., Balet, B., Brusati, M., et al., Europhys. Conf. Abstracts (Proc. 18th European Conference on Controlled Fusion and Plasma Physics), EPS, Berlin, Vol. 15C, Part I, (1991) 185.

[14] Kadomtsev, B.B., Sov. J. Plasma Phyics, vol. 1, no. 5 (1975) 389.

[15] Stubberfield, P.M., Balet, B., Cordey, J.G., et al., Europhys. Conf. Abstracts (Proc. 19th European Conference on Controlled Fusion and Plasma Physics), EPS, Innsbruck, Vol. 16C, Part I, (1992) 63.

[16] von Hellermann, M.G. and Summers, H.P., Rev., Sci. Inst. 63, 5132 (1992).

[17] Kardaun, O.J.W.F., Ryter, F., Stroth, U., et al., in Plasma Physics and Controlled Fusion Research 1992 Proc. 14th Int. Conf. Würzburg, Germany, IAEA-CN-56/F-1-3.

[18] Pasini, D., Summers, D.D.R., Philipps, V., et al., J. Nucl. Mater. 176 & 177 (1990) 186.

[19] Reichle, R., Summers, D.D.R. and Stamp, M.F., J. Nucl. Mater. 176 & 177 (1990) 375.

[20] Stork, D., Campbell, D.J., Clement, S., et al, Europhysics Conf. Abstracts (Proc. 18th European Conference on Controlled Fusion and Plasma Physics), EPS, Berlin, Vol. 15C, Part I (1991) 351.

[21] Goldston, R.J., Plasma Phys. and Control. Fusion 26 (1984) 87.

[22] Schissel, D.P., DeBoo, J.C., Burrell, K.H., et al., Nuclear Fusion 31 (1991) 73.

[23] Nave, M.F. Borba, D., Cripwell, P., et al., Europhys. Conf. Abstracts (Proc. 19th European Conference on Controlled Fusion and Plasma Physics), EPS, Innsbruck, Vol. 16C, Part I, (1992) 439.

[24] Troyon, F., Gruber, R., Saurenmann, H., et al., Plasma Phys. and Control. Fusion 26 (1984) 209.

[25] Romanelli, F.,Physics Fluids B1 (1989) 1018.

[26] Jackson, G.L., Winter, J., Taylor, T.S., et al., Phys. Fluids B4, 1, July 1992.

[27] O'Brien, D.P., Lao, L., Solano, E.R., et al., JET-P(91) 50, 1992.

[28] Bishop, C.M. Nucl. Fusion 26 (1986) 1063.

[29] Cheng, C.Z., Phys. Fluids B3 (1991) 2463 and references therein.

[30] Kerner, W., et al, European Conference on Controlled Fusion and Plasma Phys, Lisbon, 1993.

[31] Betti, R., and Freidberg, J.P., Phys. Fluids B4, 1465 (1992).

[32] Cottrell, G.A., Bhatnagar, V.P., da Costa, O., et al., "Ion Cyclotron Emission measurements during JET deuterium-tritium experiments", Nuclear Fusion, accompanying paper in this issue.

[33] Reichle, R., Campbell, D.J., Ali-Arshad, S., et al., "Termination of high performance discharges at JET", Nuclear Fusion, accompanying paper in this issue.

[34] Nave, F.N. et al., in preparation.

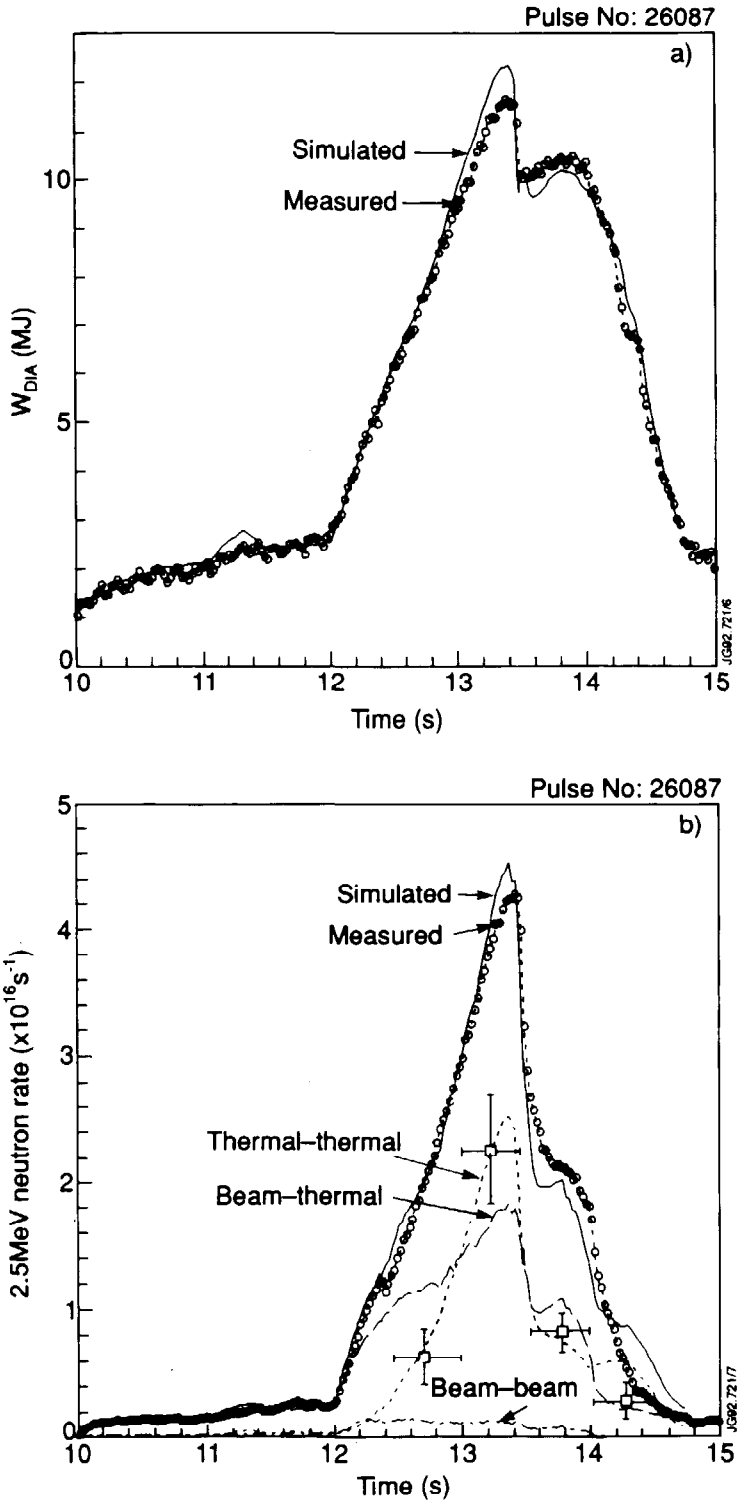

Fig. 1: Consistency checks of a TRANSP simulation for the hot-ion H-mode deuterium discharge pulse no. 26087: a) diamagnetic stored energy versus time; the measured quantities are marked by symbols (o) and are known within ± 5% b) neutron rate versus time. The measured data points are marked by symbols (o) and are from the neutron detector; they are known within ± 7%. Estimates of the thermal contribution using neutron energy spectra measurements are also shown by symbols (□). The TRANSP simulation is made up of the three components from thermal-thermal, beam-thermal and beam-beam D-D fusion reactions.

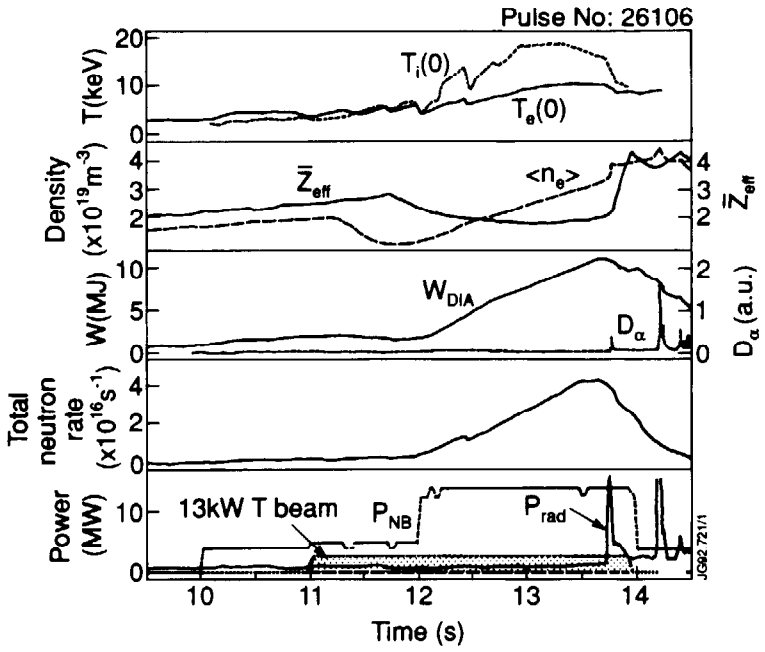

Fig. 2: The time evolution of the central electron and ion temperatures, the volume-averaged electron density, the line average $\bar{Z}_{eff}$, the plasma diamagnetic energy, the D_α emission from the edge, the total (2.5 MeV + 14 MeV) neutron rate and the neutral beam power (total and tritium) and radiated powers for pulse no. 26106.

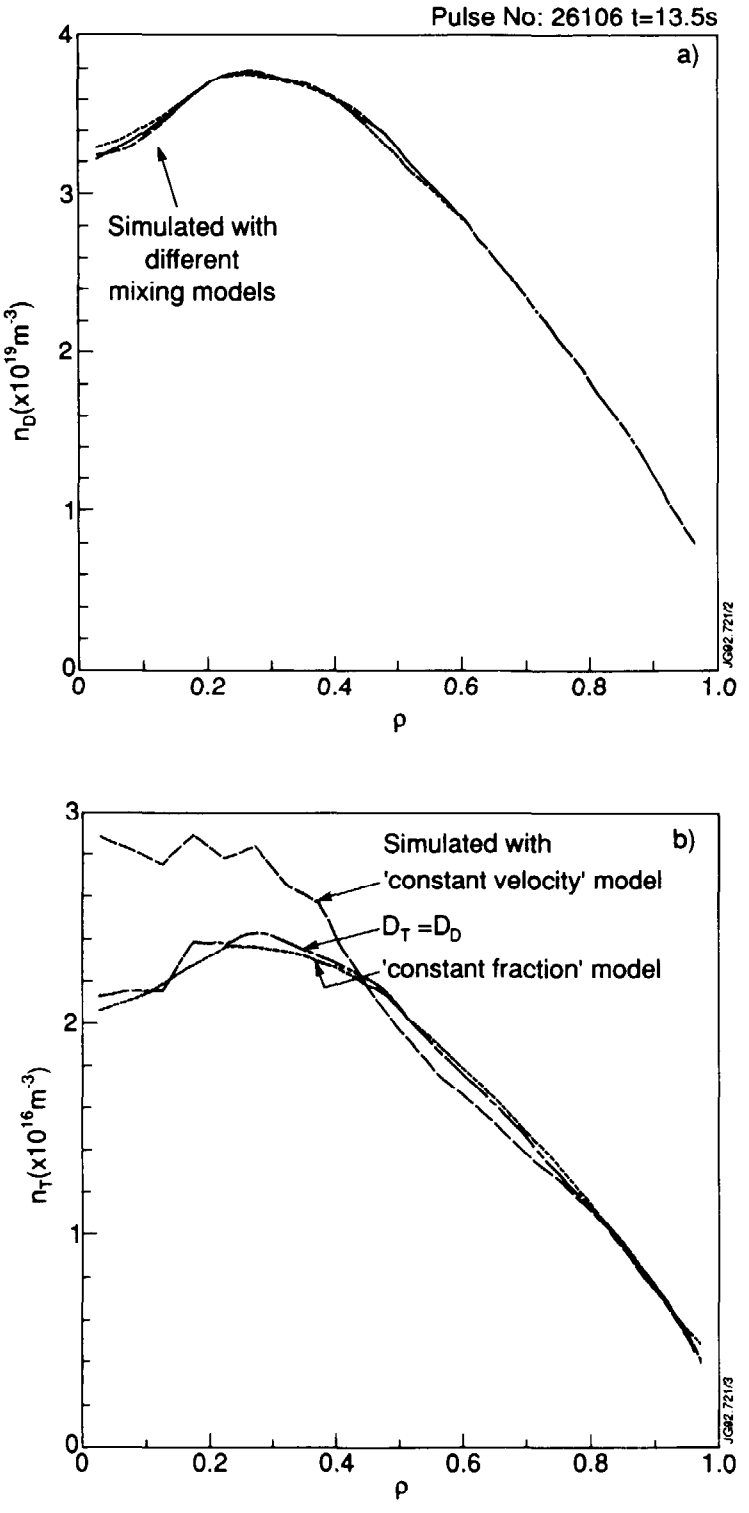

Fig. 3: * Deuterium ([a]) and tritium ([b]) density profiles from simulations with different mixing models for pulse no. 26106 at 13.5s versus normalised radius.

* *All the simulations with the "proportional diffusivities" model assume the same values for* D_T/D_D *and* v_T/v_D.

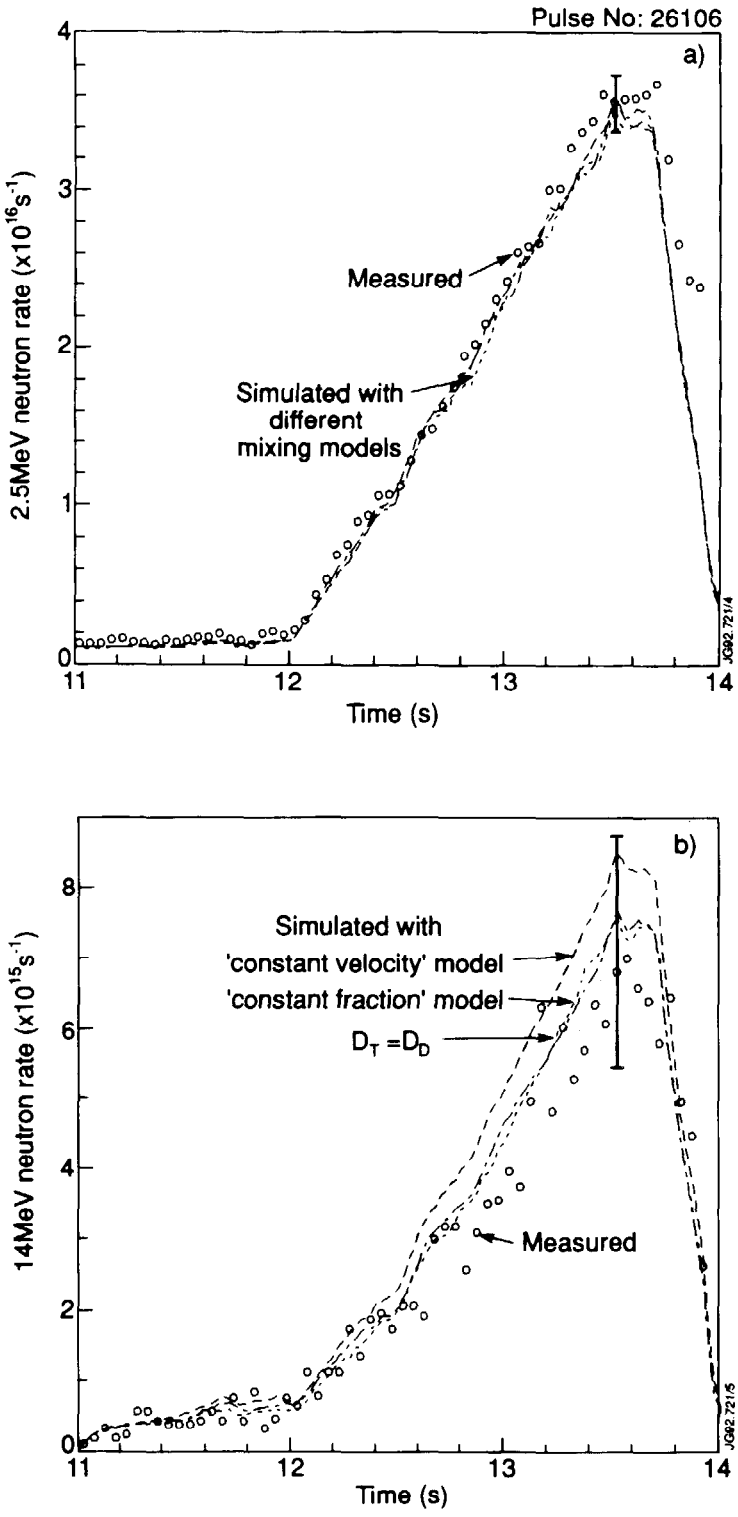

Fig. 4: * The measured and simulated rates for [a] 2.5 MeV and [b] 14 MeV neutrons for pulse no. 26106. Measured data points are marked by symbols (o).

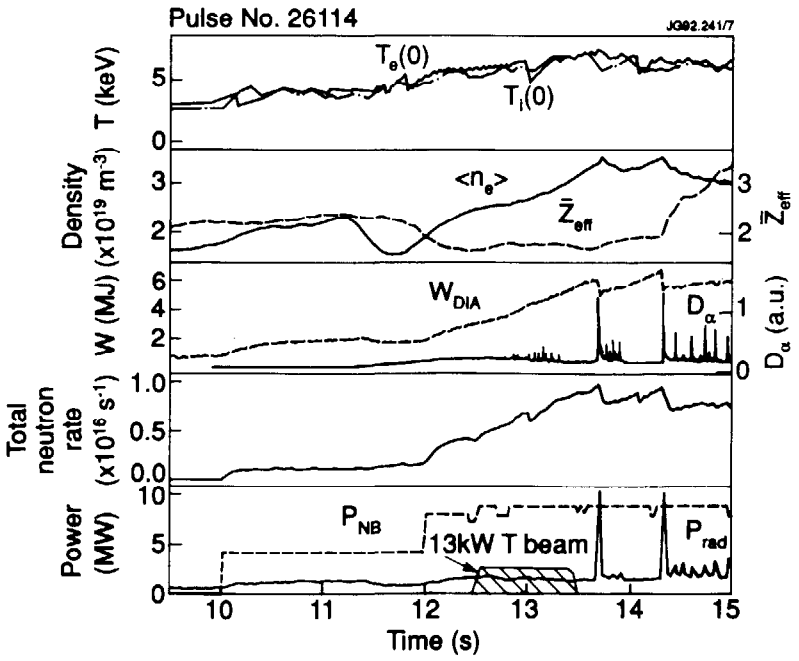

Fig. 5: The time evolution of the central electron and ion temperatures, the volume-averaged electron density, the line average $\bar{Z}_{eff}$, the plasma diamagnetic energy, the edge D_α emission, the total neutron (2.5 MeV + 14 MeV) rate and the neutral beam power (total and tritium) and radiated powers for pulse no. 26114.

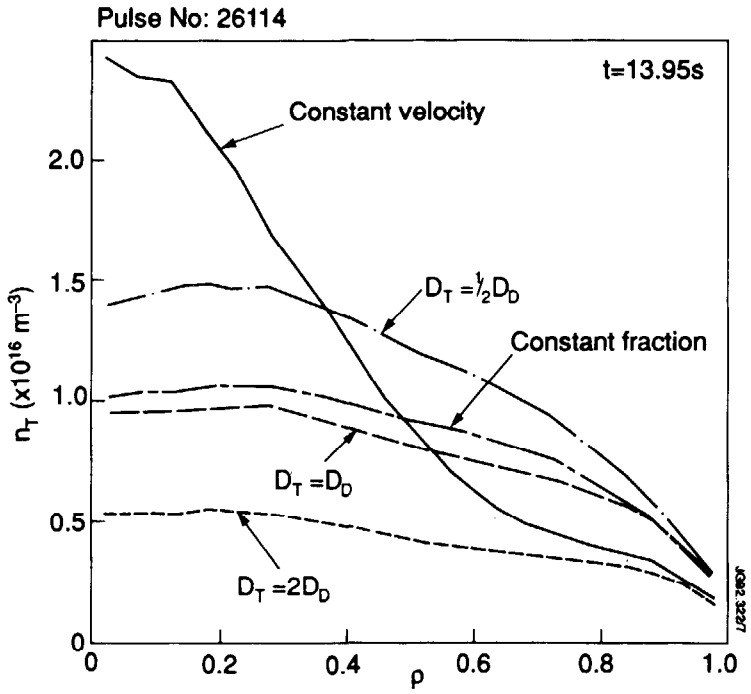

Fig. 6: * Tritium density profiles versus normalised radius simulated with different mixing models for pulse no. 26114.

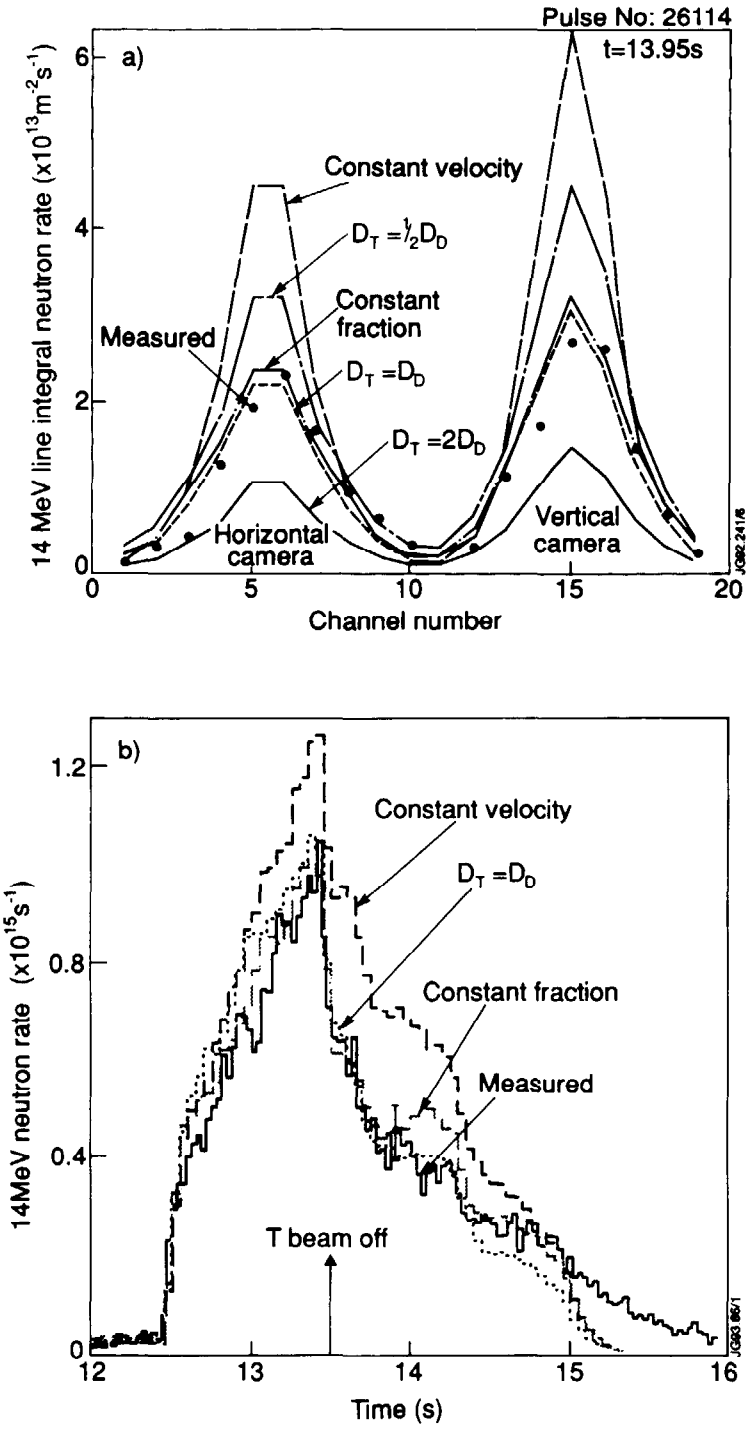

Fig. 7: * a) The measured and simulated line integral rates of 14 MeV neutrons for pulse no. 26114 at t = 13.95s (i.e. 0.45s after the tritium beam was switched off) using different mixing models.

b) Time evolution of the measured and simulated 14 MeV neutron emission rates using different mixing models.

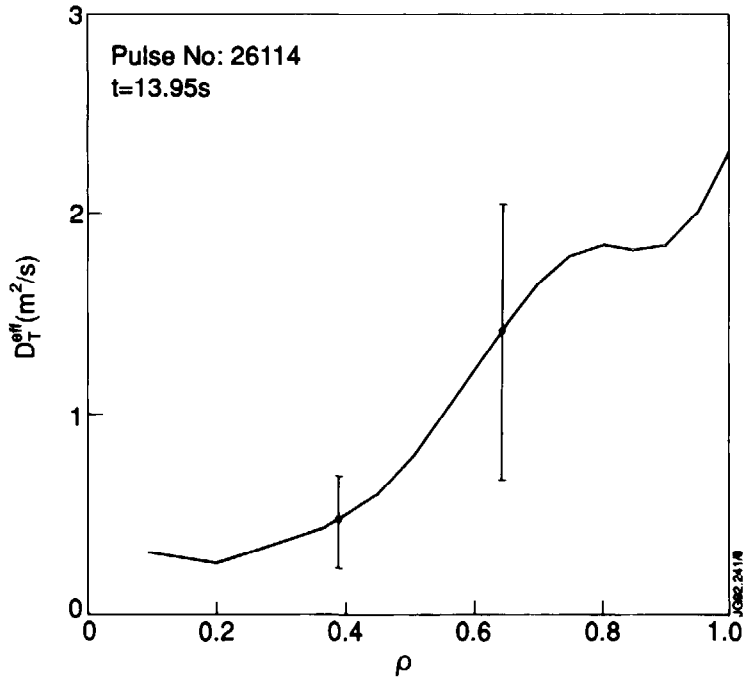

Fig. 8: The effective tritium diffusivity D_T^{eff} versus normalised radius for pulse no. 26114 at t = 13.95s.

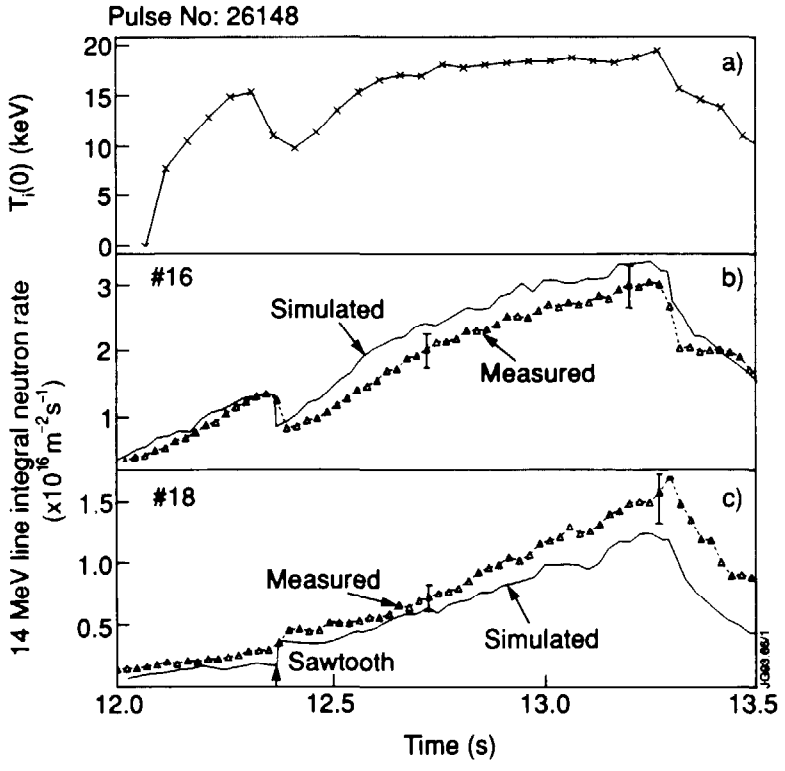

Fig. 9: The time evolution of [a] The central ion temperature from charge-exchange recombination spectroscopy; the measured and simulated 14 MeV line-integral neutron rates for [b] a central and [c] an outer neutron camera channel for pulse no. 26148. The measured data points are marked by symbols (Δ).

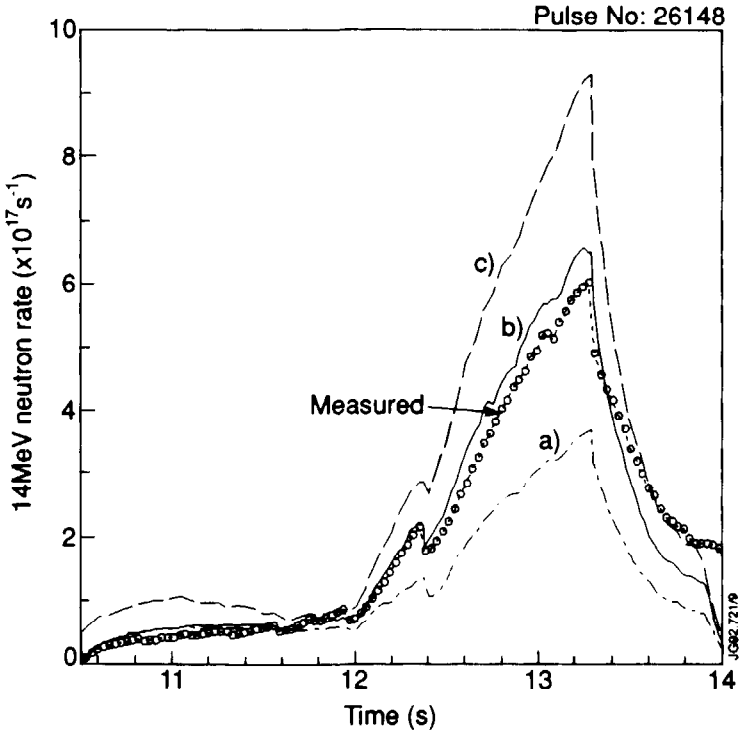

Fig. 10. The time evolution of the measured and simulated total 14 MeV rate (proportional diffusivity model $D_T/D_D = v_T/v_D = 1$) for pulse no. 26148. The measured data points are marked by symbols (o). The simulations assume: [a] all ions are recycled as deuterium, [b] the ions are recycled unchanged, [c] 20% of ions are recycled as tritium.

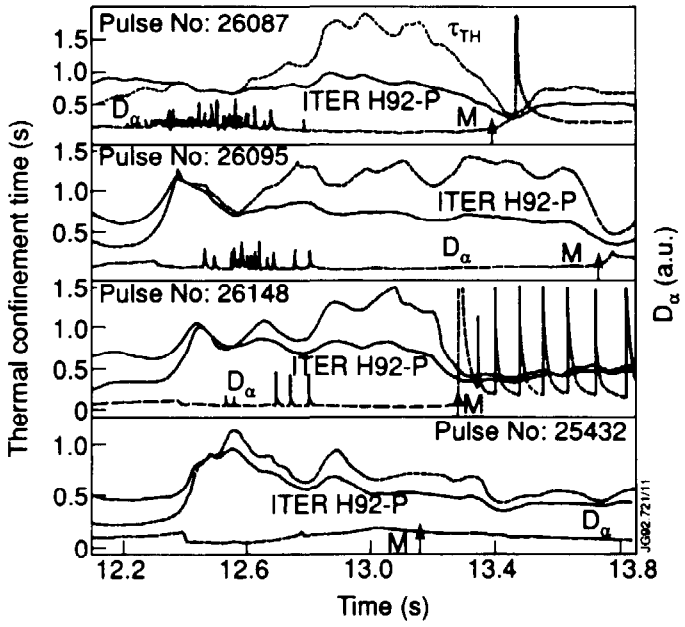

Fig. 11. The time evolution of the thermal confinement time τ_{th} compared to the value predicted by the ITERH92-P H-mode scaling expression, and the D_α emission from the edge for [a] pulse no. 26087 [b] pulse no. 26095 [c] pulse no. 26148 and [d] pulse no. 25432 (the time-axis is advanced by 1s). The letter M indicates the times of the maximum measured total neutron rate in each pulse.

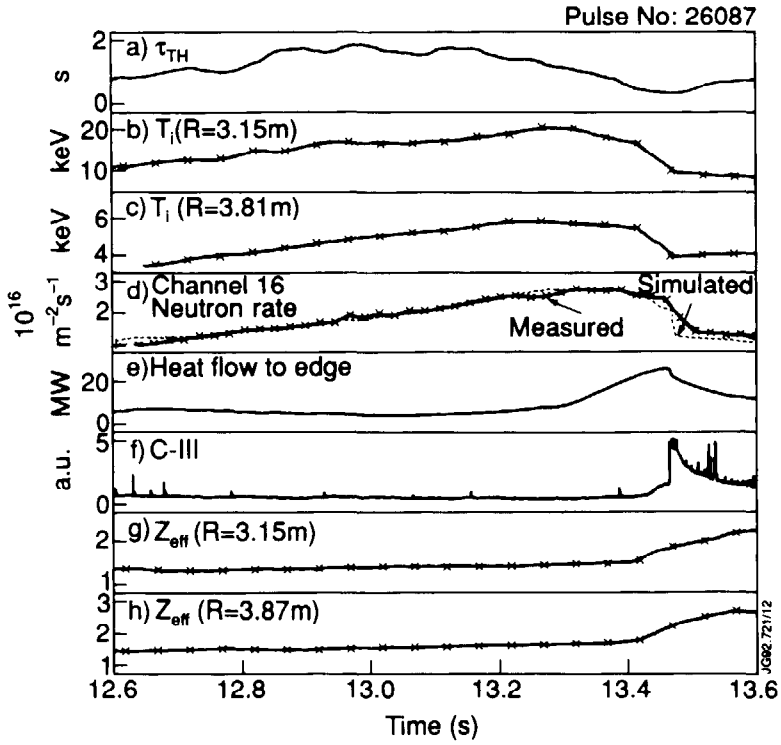

Fig. 12. The time evolution of [a] the thermal confinement time τ_{th}, [b] the central and [c] the edge values for the ion temperature, [d] the measured and simulated 2.5 MeV line-integral neutron rates for a central (# 16) neutron camera channel, [e] the calculated heat flow to the X-point target, [f] the measured C-III light emission from the edge, [g] the central and [h] the edge values for the effective charge Z_{eff} for pulse no. 26087. The symbols (x) mark the measured data points. T_i and Z_{eff} are measured by charge-exchange recombination spectroscopy.

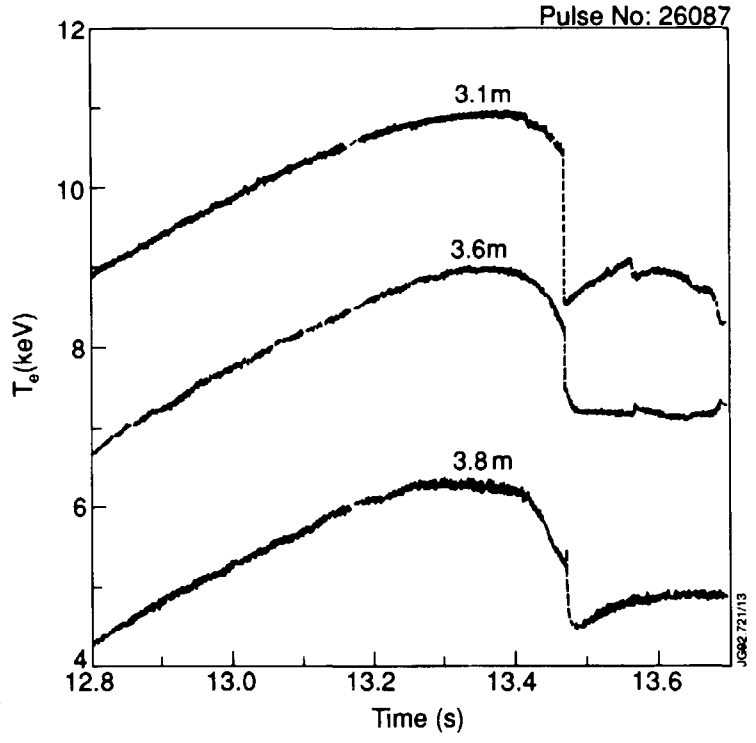

Fig. 13. The time evolution of the electron temperature T_e measured by the ECE grating polychromator at different major radius positions for pulse no. 26087.

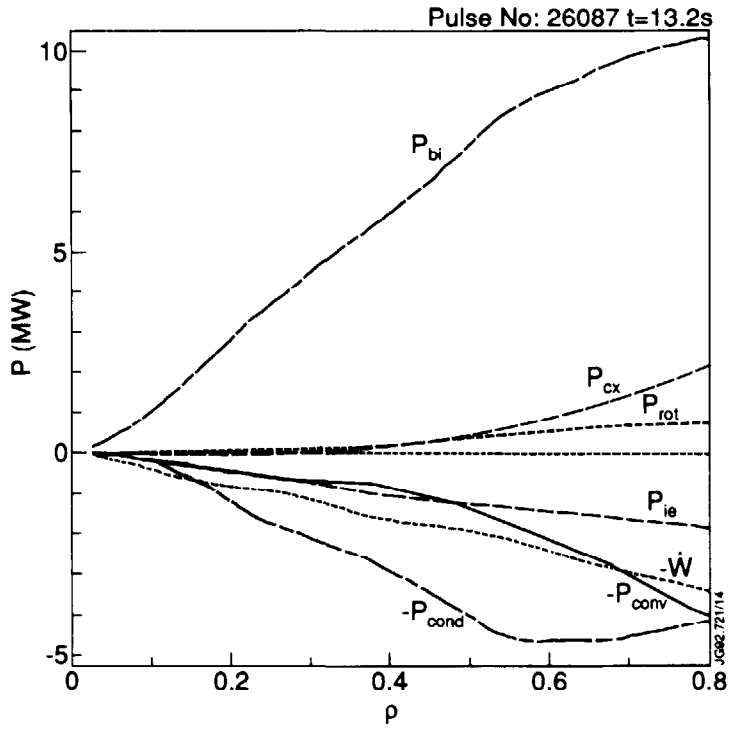

Fig. 14. Volume - integrated ion power balance versus normalised radius for pulse no. 26087 at t = 13.2s. The symbols are as follows: P_{bi}, power input to ions from fast ions, P_{rot}, power input to ions from viscous dissipation of plasma rotation, P_{conv}, power loss by convection, P_{cond}, power loss by conduction, W_i, rate of increase of ion stored energy, P_{ie}, ion-electron equipartition term, P_{CX} power loss by charge-exchange.

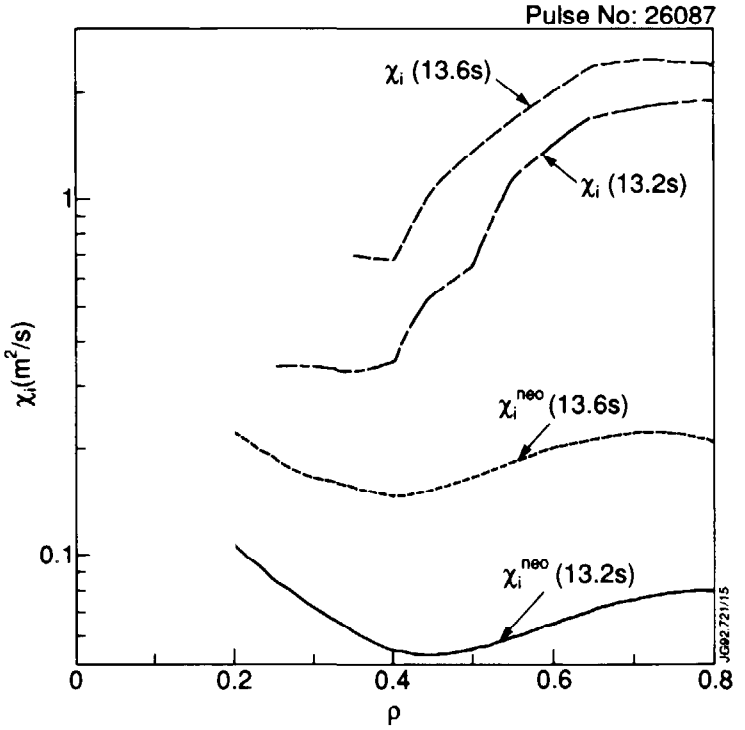

Fig. 15. Ion thermal conductivity χ_i and neoclassical prediction χ_i^{neo} versus normalised radius during (t = 13.2s) and after (t = 13.6s) the period of enhanced confinement for pulse no. 26087.

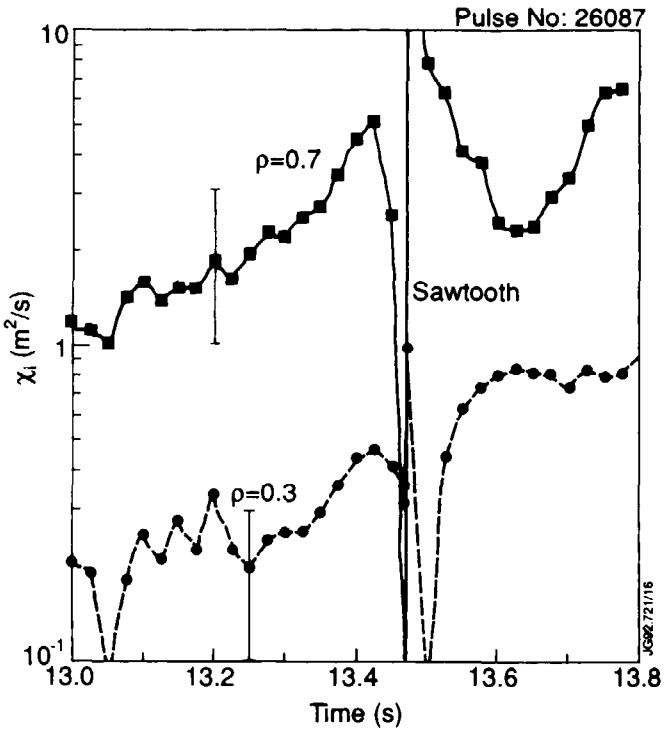

Fig. 16. The time evolution of the ion thermal conductivity χ_i at normalised radius $\rho = 0.3$ and $\rho = 0.7$ for pulse no. 26087. The symbols mark the calculation times.

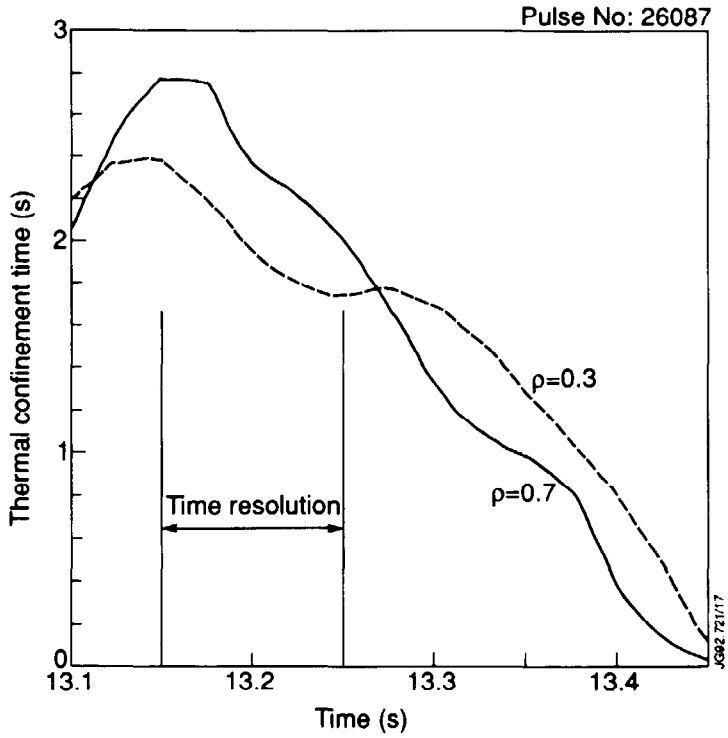

Fig. 17. The time evolution of the local thermal confinement time τ_{th} at normalised radius $\rho = 0.3$ and $\rho = 0.7$ for pulse no. 26087.

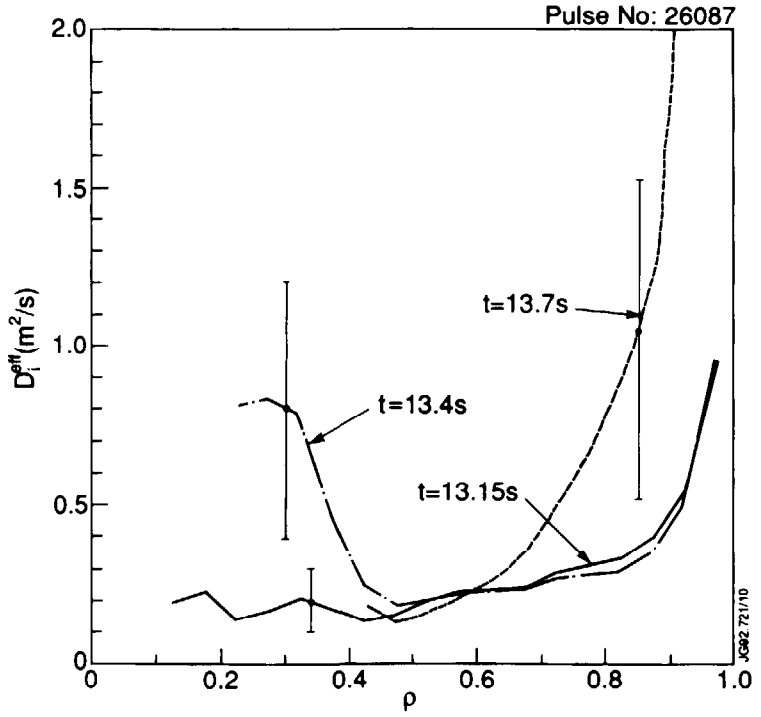

Fig. 18. The effective ion diffusivity profile D_i^{eff} versus normalised radius for pulse no. 26087 during the high performance phase (t = 13.15s), before (t = 13.4s) and after (t = 13.7s) the sawtooth crash.

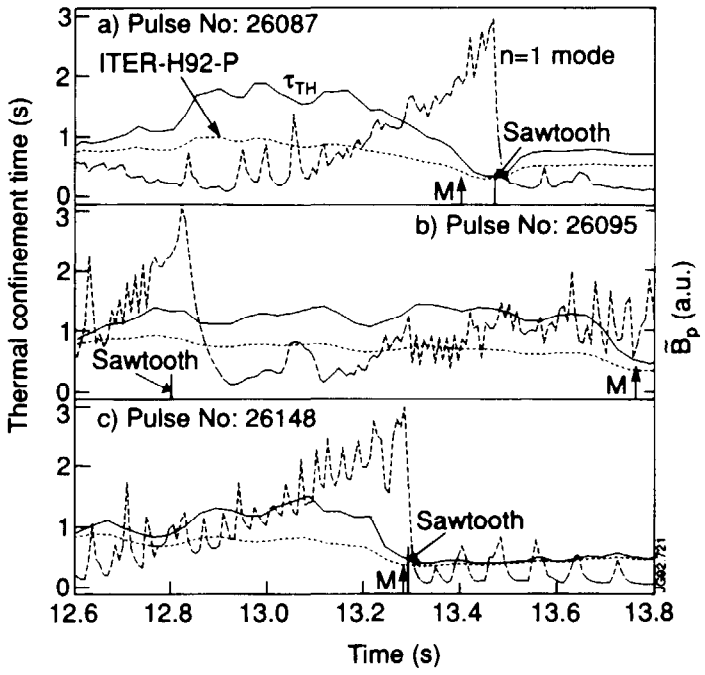

Fig. 19. The time evolution of the measured n = 1 MHD activity, thermal confinement time τ_{TH} and value of τ_{TH} predicted by ITERH92-P for a) pulse no. 26087 b) pulse no. 26095 and c) pulse no. 26148. The letter M indicates the times of maximum measured total neutron rate.

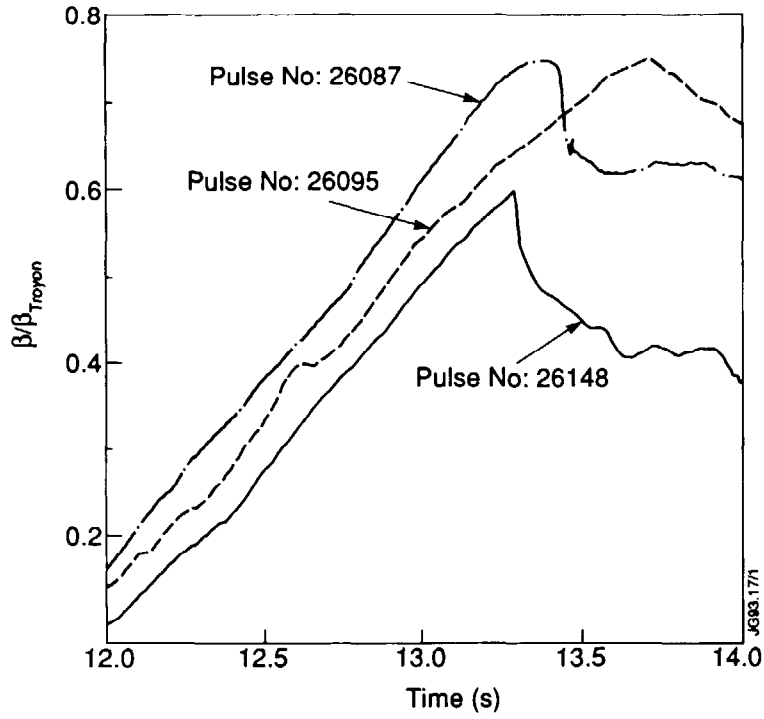

Fig. 20. The ratio of beta calculated by TRANSP as a function of time for pulse numbers 26087, 26095 and 26148 normalised to β_{TROYON} (%) = $g_n u_o I_p(MA)/B_T(T)\, a(m)$ where I_p is the total plasma current, B_T the toroidal field, a is the horizontal minor radius, $g_n = 2.2$ and $\mu_o = 0.4\pi$ in these units.

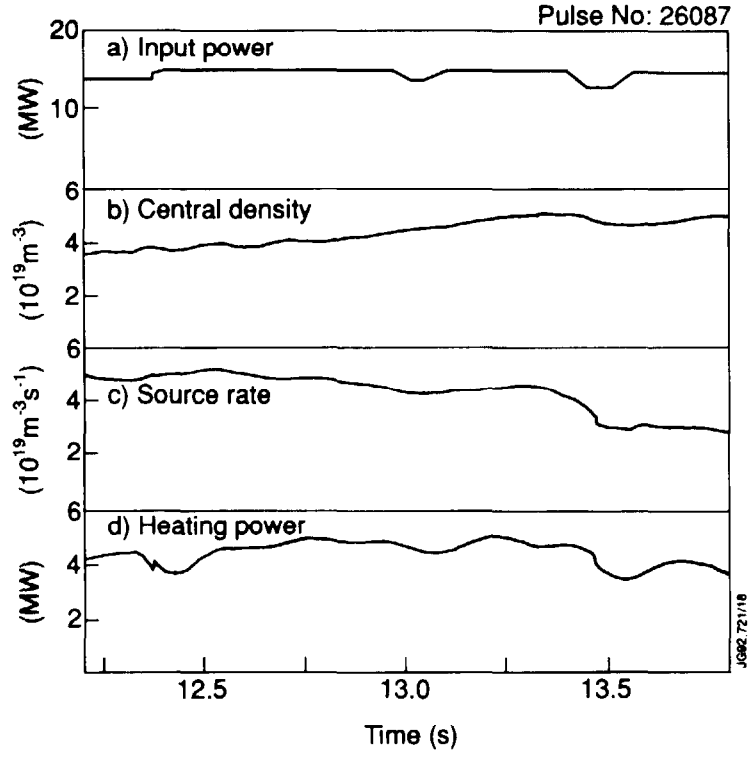

Fig. 21. The time evolution of [a] the total neutral beam input power, [b] the central electron density, [c] the central fast ion source rate and [d] the heating power to the central third of the plasma for pulse no. 26087.

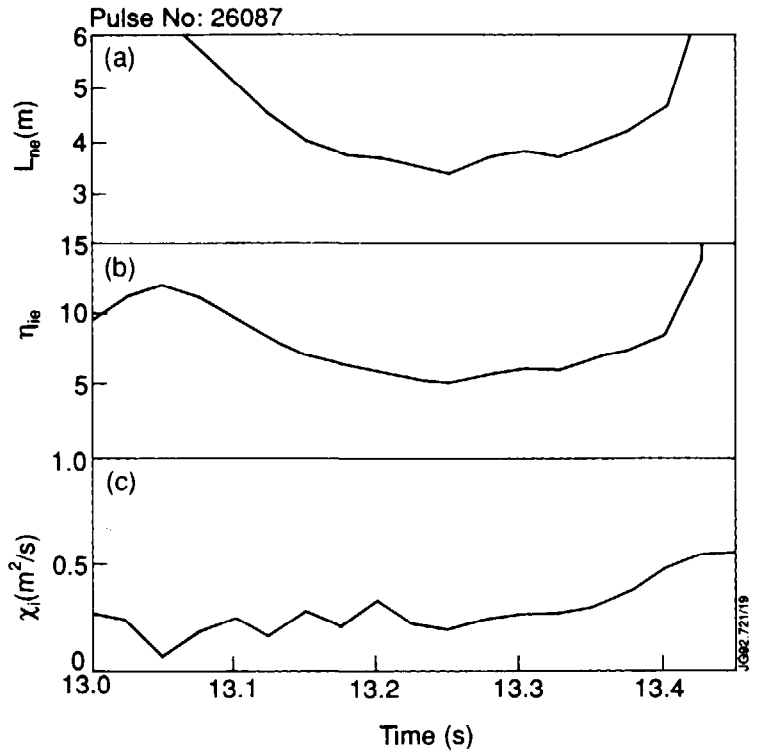

Fig. 22. The time evolution of [a] the electron density scale length $L_{ne} = - ne/\nabla n_e$, [b] The ratio of electron density and ion temperature scale lengths $\eta_{ie} = \frac{L_{ne}}{L_{Ti}}$, and [c] the ion thermal conductivity χ_i at a normalised radius $\rho = 0.3$ for pulse no. 26087.

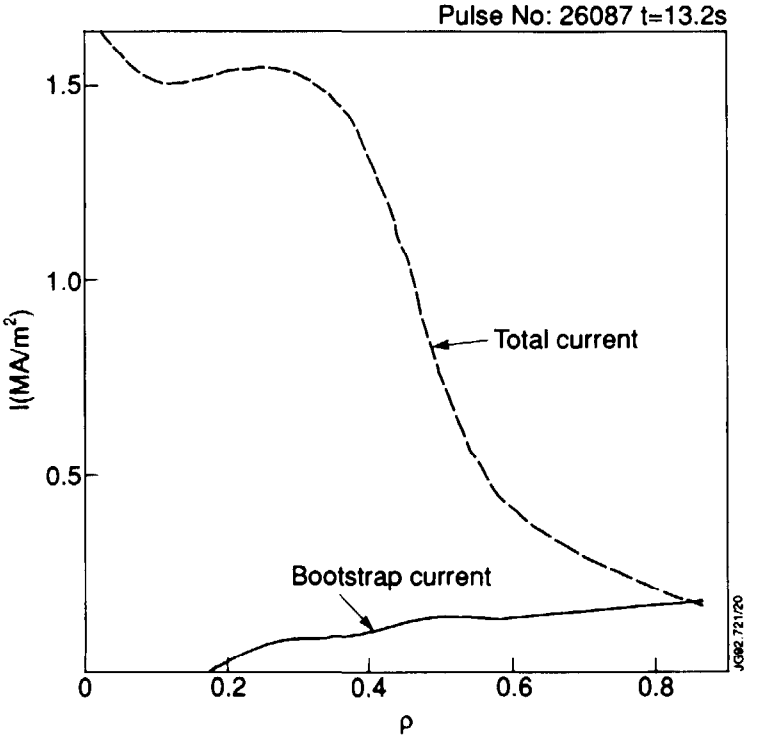

Fig. 23. The total current and bootstrap current versus normalised radius at t = 13.2s for pulse no. 26087.

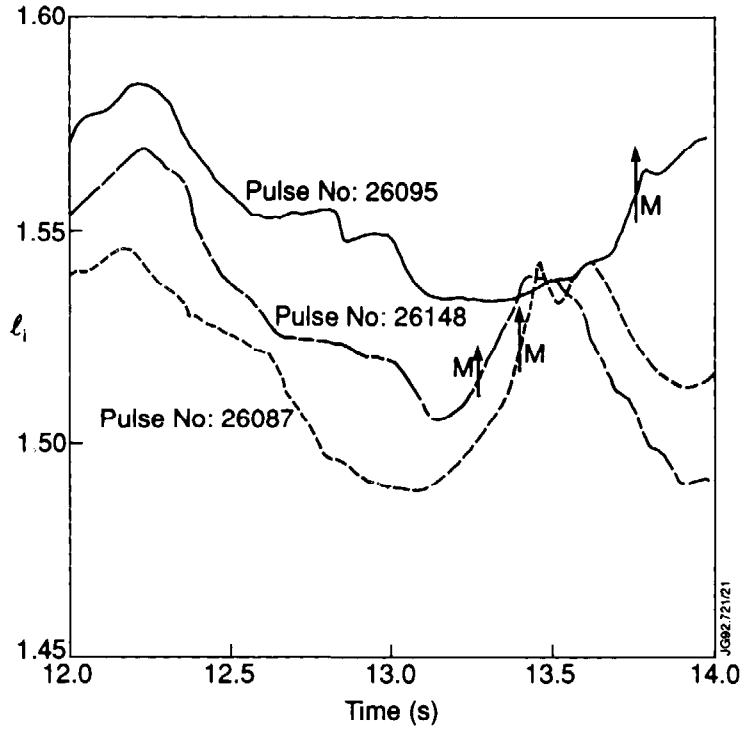

Fig. 24. The time evolution of ℓ_i for pulse numbers 26087, 26095 and 26148. The letter M indicates the times of the maximum neutron yield.

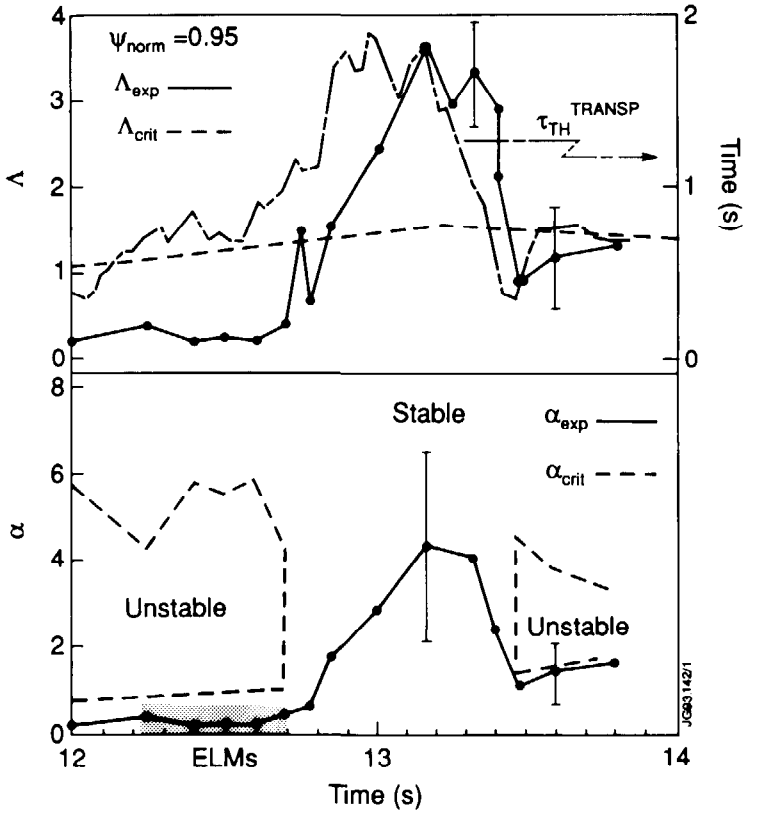

Fig. 25. a) the time evolution of Λ_{exp} and Λ_{crit} (see text) and the thermal confinement time τ_{th} and b) marginally stable boundaries for ballooning for pulse no. 26087.

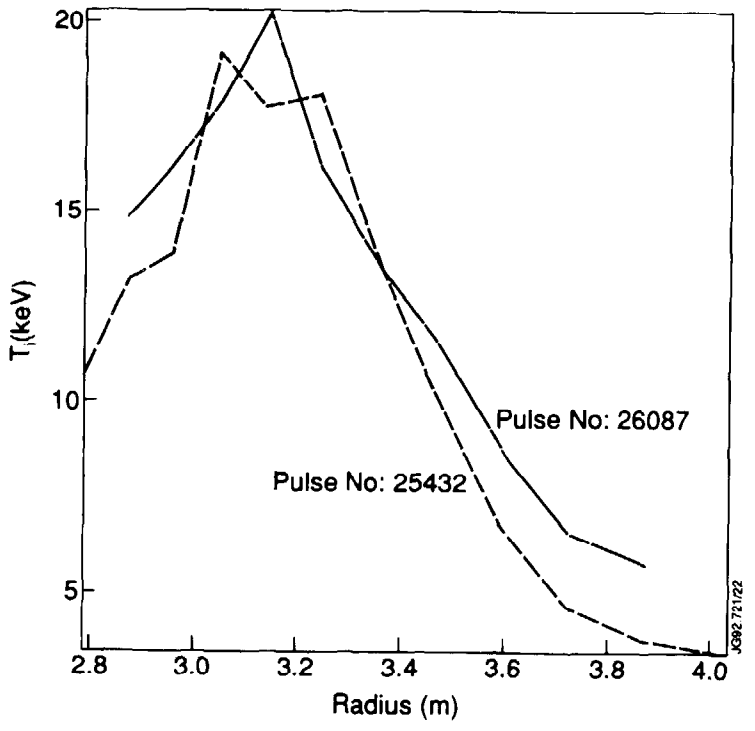

Fig. 26. Measured ion temperature profiles versus major radius for pulse numbers 26087 and 25432, 100 ms before time of maximum measured total neutron yield.

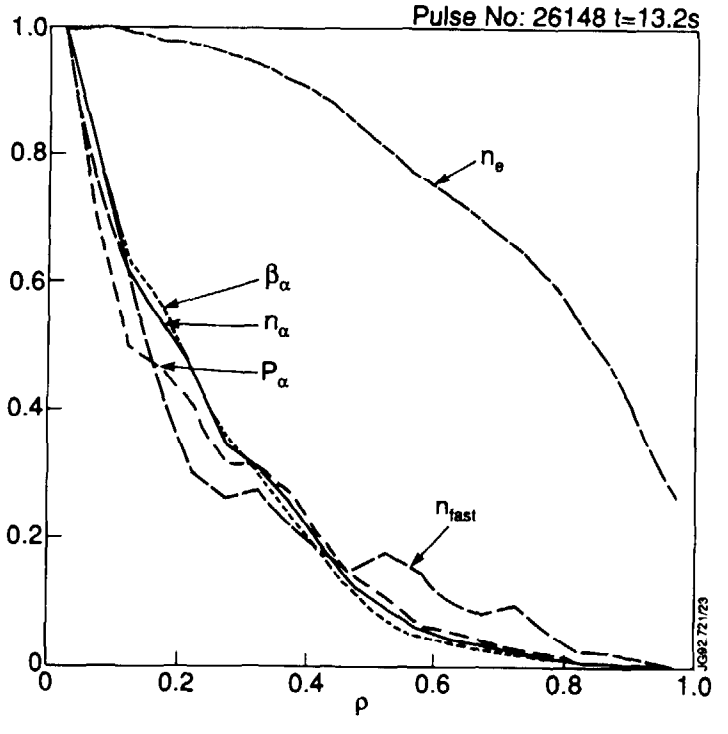

Fig. 27. The normalised electron density n_e, α-particle density n_α, toroidal α-particle beta β_α, total α-particle heating rate P_α and fast ion density n_{fast} versus normalised radius at t = 13.2s for pulse no. 26148. See Table II for normalisation factors.

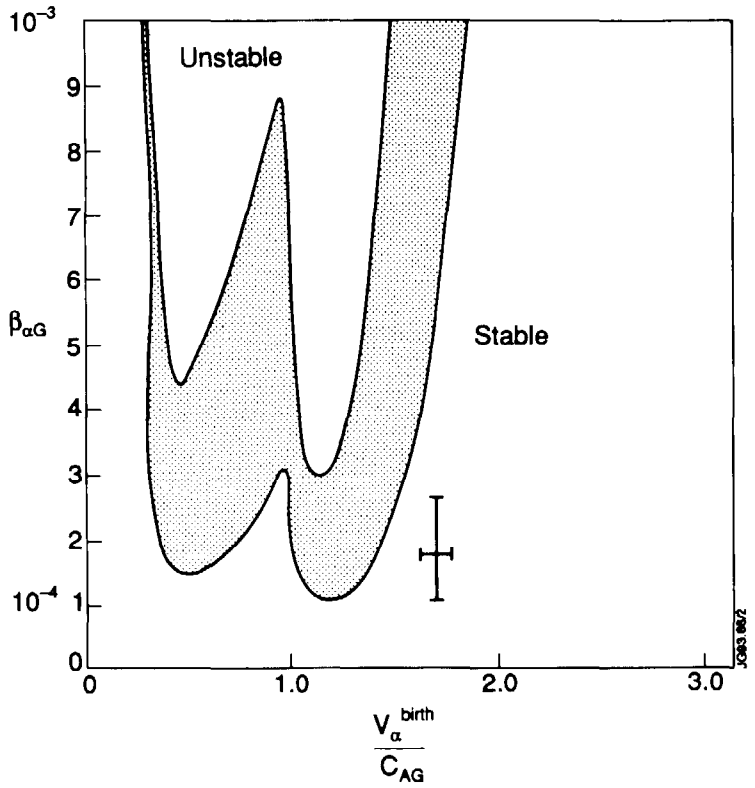

Fig. 28. Stability boundary for the TAE mode with n = 4, m = 3, 4 at the time of maximum $\beta_{\alpha G}$ (pulse no. 26148). Parameters at the $q_G = 7/6$ surface are as follows: $r_G/a = 0.47 \pm 0.04$; $n_e = (3 \pm 0.3) \times 10^{19}$ m^{-3}; $n_D = (1.8 \pm 0.2) \times 10^{19}$ m^{-3}; $n_T = (2.0 \pm 0.2) \times 10^{18}$ m^{-3}; $n_{imp} = (2.0 \pm 0.2) \times 10^{18}$ m^{-3}; $T_i = (11 \pm 1)$ keV; $T_e = (7.5 \pm 0.5)$ keV; $L_\alpha/a = 0.15 \pm 0.5$; $\beta_{\alpha G} = (1.7 \pm 0.7) \times 10^{-4}$; $B_T = 2.8$T. We have assumed $T_i = T_D = T_T$. The hatched region reflects the sensitivity of the marginal stability curve to variations of the relevant parameters within the corresponding error bars. Also shown in the figure are the values of $\beta_{\alpha G}$ and v_α^{birth}/C_{AG} at the selected time.